Witteveen + Bos

Universiteit Utrecht

Witteveen+Bos
Universiteit Utrecht

Leak detection at underground building sites

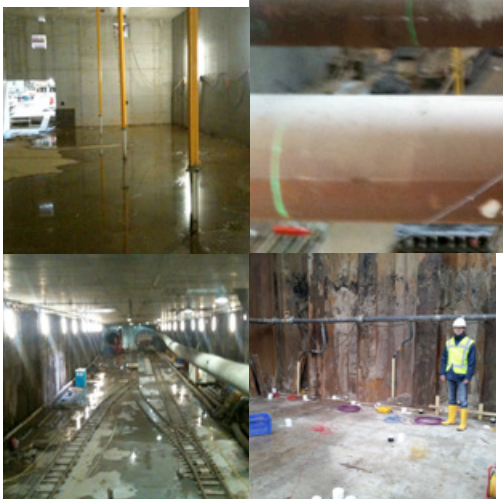

Witteveen+Bos

Universiteit Utrecht

Leak detection at underground building sites

project	project code W+B	status
MSc Thesis	ZZWM6500-13	final version
author	**student number**	**date**
J. Vleghaar	3361225	28 January 2013

authorization	name	initials
approved	Ir. T.H. van Wee (W+B)	
approved	Prof. dr. R.J. Schotting (UU)	

Witteveen+Bos
Van Twickelostraat 2
P.O. Box 233
7400 AE Deventer
The Netherlands
telephone +31 570 69 79 11
fax +31 570 69 73 44
www.witteveenbos.com

The Quality management system of Witteveen+Bos has been approved based on ISO 9001.

INDEX **p.**

1. ABSTRACT

Imperfections in water resistant screens surrounding an underground building site can cause the occurrence of a leakage as a consequence of an artificially lowered groundwater level at this site. Leakages in a water resistant screen can be detected by active or passive testing methods. An active testing method is presented in which piezometer measurement data from a pumping test are used for characterizing the diaphragm wall of Vijzelgracht Station in Amsterdam. The conditions under which such a pumping test must be performed are highly demanding and are generally not met in practice. Hereafter, a passive testing method is presented in which the configuration of piezometers outside the building site is optimized in order to timely localize an occurring leakage by spatially interpolating their measurement data. This analysis is done for several values for aquifer properties and leakage discharge. The procedure results in an optimal piezometer configuration, namely a row of piezometers parallel to the building site for all scenarios tested. The optimal distance from this row to the site and the optimal mutual distance between piezometers depend on the aquifer properties. Subsequently, this method is applied in a case study at Vijzelgracht Station, confirming the use of the method. Finally, an active method for leakage detection using geoelectrical measurements is presented. As a case study, this method is applied to the sheet piling at a building site in the province of Overijssel in the Netherlands.

Key words: water resistant screen, diaphragm wall, sheet piling, leakage, pumping test, piezometer, optimization, geoelectrical measurements.

2. INTRODUCTION

2.1. Relevance of this thesis

When building underground civil technical constructions, a lowered groundwater level at the building site is required in order to dig under dry conditions. Underground building sites therefore have to be enclosed by water resistant screens so that a highly reduced groundwater level can be achieved while affecting the surrounding groundwater levels as little as possible. Commonly used types of screens are diaphragm walls and sheet pilings. Leakages in such screens can occur due to imperfections in it, which may cause flooding inside the building site and lowered groundwater levels in the area surrounding it.

Leakages at underground building sites are a common phenomenon. Notorious leakages are, for example, the ones that occurred during the construction of the North South Line, a metro line in Amsterdam. Six stations are built for this line, three of which are deeply excavated and enclosed by diaphragm walls. At Vijzelgracht Station, which is one of these deep stations, major leakages occurred in 2008. As a consequence, groundwater levels below buildings neighboring the site severely dropped, causing damage to these buildings by subsidence.

Multiple risks due to leakages can be distinguished. Besides the risk of damage to the area surrounding a building site, also the progress of the proceedings may be at stake. The risk of damage to neighboring buildings especially applies in densely built areas while the risk of delay can be found at any building site. The events at Vijzelgracht Station in 2008, among others, have caused a severe financial loss, delay to the proceedings of the station and reputational damage to the authorities, companies and the North South Line project as a whole.

2.2. Purpose of this thesis

The risk of damage or delay to proceedings due to leakages is inherent to building at underground sites, so it is relevant to timely observe and localize leakages in water resistant screens like a diaphragm wall or a sheet piling. Testing the watertightness of screens can be done actively or passively. Actively testing a screen implies that a field experiment is set up and its results are analyzed. Passively testing implies that the state of a building site is continuously observed so that timely intervention is possible when a leakage occurs. The research presented in this thesis aims at providing tools for leak detection in water resistant screens using piezometer data and geoelectrical measurements.

The research questions that are answered in this thesis are:

1. What method can actively test the state of the diaphragm wall of Vijzelgracht Station using piezometer data?
2. What piezometer configuration is optimal for localizing a theoretical leak in a diaphragm wall?
3. What piezometer configuration is optimal for localizing a theoretical leak in the diaphragm wall of Vijzelgracht Station?
4. How can geoelectrical measurements be used to actively test the watertightness of a water resistant screen?

2.3. Reading guide

Chapter 3 discusses some theoretical aspects which are relevant for subsequent chapters. Research questions 1 through 4 are the topics of Chapters 4 through 7 respectively. The answer to each research question can be found in the conclusion section of each respective chapter.

3. THEORETICAL ASPECTS

3.1. Constructing a diaphragm wall

Diaphragm walls consist of elements of ferroconcrete which have a typical width of 2 to 5 meters, a typical thickness of 1 to 1.5 meters and a depth up to several tens of meters. The construction of an element of a diaphragm wall is shown in Figure 3.1.

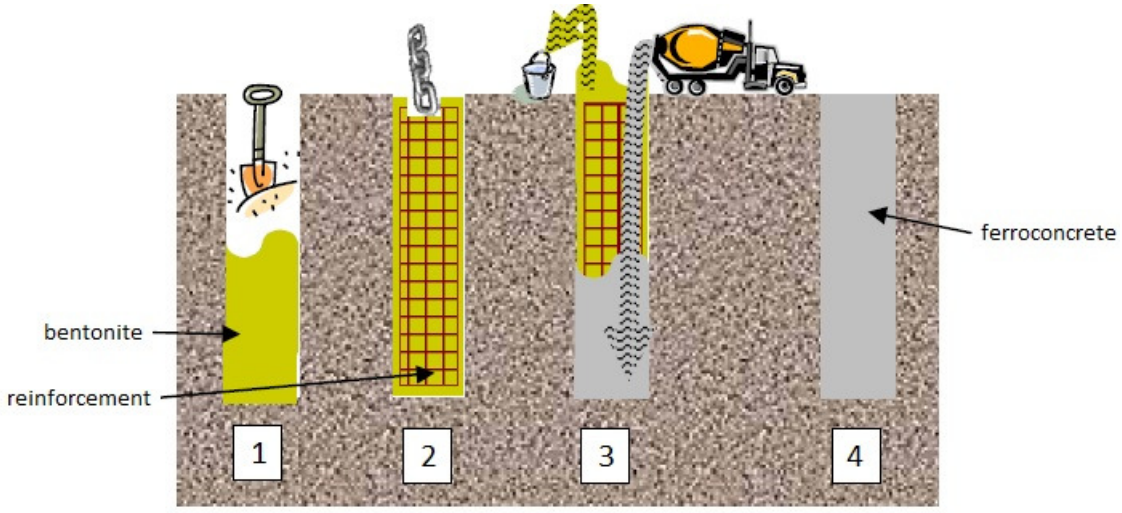

Figure 3.1. Construction of a diaphragm wall element (Dijk, 2008).

The first step when constructing a diaphragm wall element is digging a slot (Figure 3.1.1). The slot is filled with bentonite to prevent it from collapsing and to prevent nearby buildings from settling due to subsidence of underground layers. Bentonite is a naturally occurring type of clay that can easily absorb water and it is watertight when mixed with water. It also has a thixotropic property (Dijk, 2008), which implies that it is in a liquid phase when in motion, but it is in a solid phase when in rest. After filling the slot with bentonite, an iron reinforcement is put into the bentonite (Figure 3.1.2) to increase the strength of the final diaphragm wall. Finally, the slot is filled with concrete from below (Figure 3.1.3), replacing the bentonite, which is intercepted and purified for reuse. Now this element of the diaphragm wall is finished (Figure 3.1.4) and the next element can be constructed. A so-called stop-end is constructed at the end of each element of the diaphragm wall. This is a steel profile with some rubber binding in it. The steel profile is removed after the construction of the opposite diaphragm wall element, leaving the rubber binding which makes the joint between two elements of the diaphragm wall watertight (Dijk, 2008).

The building site at Vijzelgracht Station has a length of 254 meter and it has a width of 19 meters. Its circumference is therefore 546 meter, so this length of diaphragm wall had to be constructed. It consists of 114 elements, so the average width of an element of the diaphragm wall is 4.79 meter. The thickness of the elements varies from 1.2 to 1.5 meter and the bottom of each element is at NAP-45 meter (Dijk, 2008). The soil structure and geohydrological parameters for Vijzelgracht Station are shown in Table 3.1 (Duineveld, 2009; Salet, 2010).

Layer	**Depth (m below NAP)**		**Name/material**	**Geohydrological parameter**
	from	*to*		
1	0	-3	sand	k=5 m/day
2	-3	-6.5	clay	c=500 days

3	-6.5	-9	sand	k=5 m/day
4	-9	-12	clay	c=4000 days
5	-12	-14	first sand layer	k=30 m/day
6	-14	-17	alleröd	c=25 days
7	-17	-25	second sand layer	k=30 m/day
8	-25	-41	clay	c=3500 days
9	-41	-43	'tussenzandlaag'	k=0.3 m/day
10	-43	-50.5	clay	c=3500 days
11	-50.5	-55	third sand layer	k=30 m/day

Table 3.1. Soil structure and geohydrological parameters at Vijzelgracht Station.

3.2. The occurrence of leakages in a diaphragm wall

Leakages in a diaphragm wall usually occur at the transition between its elements. A leakage at such a transition may occur due to the absence or careless construction of a stop-end between these elements. A moderate leakage caused by the absence of a stop-end resulted at Vijzelgracht Station in the 'tussenzandlaag', which is between NAP-40 meter and NAP-41.5 meter. The construction of a stop-end up to this depth was infeasible (Bhageloe, 2004). On June 19th 2008, a major leakage occurred at Vijzelgracht Station at about NAP-12 meter because, among other causes, a stop-end was left between elements of the wall (Salet, 2008).

A leakage may also occur due to irregularities in the diaphragm wall, like inclusions of sand or bentonite in concrete (Jonker, 2010). These inclusions arise during the construction of the wall. Bentonite inclusions occur when concrete does not fully replace the bentonite during construction (see Figure 3.1.3). Such inclusions usually occur near or on the edge of a wall element. Bentonite can flow into a joint between the stop-end and the edge of a completed wall element during the construction of an adjacent element (Salet, 2008). This bentonite is left behind when the stop-end cannot be removed. Also, bentonite may remain attached to a stop-end during concreting. A bentonite inclusion is not causing a leakage before the excavation of a building site starts, since it is solid and watertight in this situation. But a bentonite inclusion may become a weakness when it dries during excavation, possibly combined with vibrations due to the proceedings. It eventually may shrink, rupture or flow out of the wall (Jonker, 2010; Salet, 2008), possibly carrying some sediment so that the resulting opening is even larger than the original inclusion.

3.3. Testing the state of a diaphragm wall by analytical methods

Pujades et al. (2012) have set up an analytical method to test the state of a diaphragm wall framing a linear building site, like Vijzelgracht Station. They use drawdown measurements in one or more piezometers located inside the building site during a pumping test. Figure 3.2 shows the excavation site cross section. In this figure, d_{dw} indicates the width of the excavation site and w_{dw} indicates the thickness of the diaphragm wall.

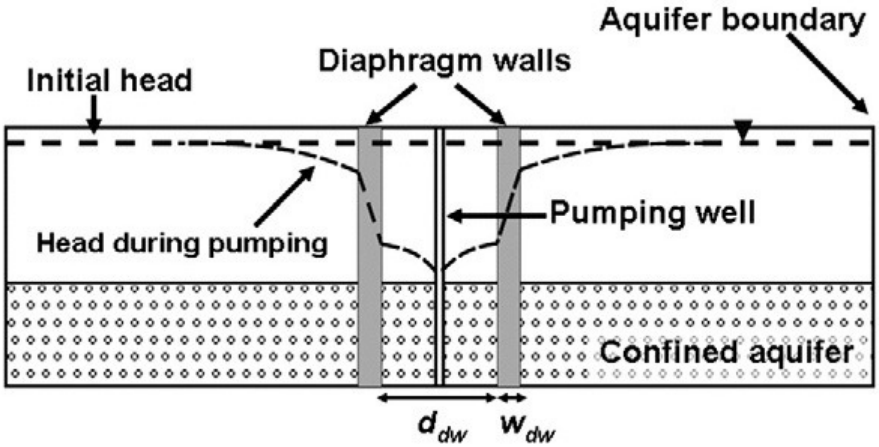

Figure 3.2. Excavation site cross section (Pujades et al., 2012). d_{dw} indicates the width of the excavation site, w_{dw} indicates the thickness of the diaphragm wall.

The basic idea underlying this method is that drawdown measurements in a particular piezometer inside the building site indicate a change in flow behavior over time during the pumping test. This change in flow behavior over time is shown in Figure 3.3, which is a top view of the excavation site. The time indications shown are discussed when applied. The change in flow behavior is determined by the state of the diaphragm wall. The method requires the use of only one pumping well so that drawdown measurements from piezometers located inside the building site can be attributed to the discharge from this specific well. Also, it is required that either the discharge rate from the pumping well or the head in the pumping well is fixed.

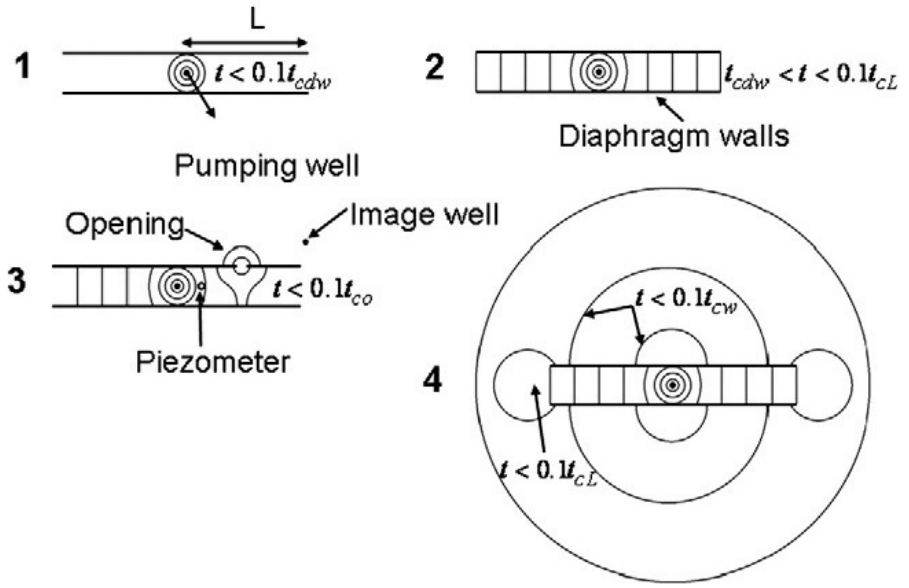

Figure 3.3. Top view of flow behavior evolution over time (Pujades et al., 2012).

When the pumping test has just started (Figure 3.3.1), the cone of depression has not yet reached the diaphragm walls, so a piezometer nearby the pumping well will indicate radial flow behavior. In some later stage, the cone has reached the walls (Figures 3.3.2 and 3.3.3) but water is still preferably discharged from inside the excavation site since it has less resistance by doing so. The flow behavior observed in the piezometer has now changed from radial flow to linear flow. In the latest stages of the pumping test (Figure

3.3.4), increasing volumes of water enter the building site through openings in the diaphragm walls because the head gradient over the walls has become large. A steady state condition will usually be reached at even later times (Pujades et al., 2012).

When the drawdown data obtained are plotted against time, some indications on the state of the diaphragm wall are observed (Pujades et al., 2012). But before doing so, these data have to be modified by a few calculation steps. First, both drawdown (s) and time (t) are written in dimensionless form, denoted by d.u. (dimensionless unit). This is done by dividing the measurement values by some characteristic values, given in Table 4.1. After this, the derivative of dimensionless drawdown is taken with respect to the natural logarithm of time. This dimensionless logarithmic derivative is denoted by s' (d.u.) and is defined by

$$s' = \frac{\partial s}{\partial \ln(t)} = t\frac{\partial s}{\partial t} \qquad (3.1)$$

A plot of s' versus time is called a diagnostic plot. Renard et al. (2008) propose the use of diagnostic plots for interpreting the results of a pumping test. They do so because changes in drawdown evolution are much more sensitive to the logarithmic time derivative compared to the normal time derivative. Trends in drawdown are therefore more easily recognized in diagnostic plots. Renard et al. (2008) also discuss some typical diagnostic plots corresponding to a specific hydrogeological field situation.

A theoretical result from the diagnostic plot by Pujades et al. (2012) is shown in Figure 3.4. Again, time indications in this figure are discussed when applied. The diagnostic plot is shown together with the theoretical results for the evolution of purely radial and purely linear flow. Pujades et al. (2012) use the following expressions for theoretical radial and linear flow.

Radial flow: $$h(r) = \frac{Q_p}{2\pi T_{aq}} \ln \frac{r}{R} \qquad (3.2)$$

In which: $$R = \sqrt{\frac{2.25 T_{aq} t}{S_{aq}}} \qquad (3.3)$$

Linear flow: $$q* = 2 s_p \sqrt{\frac{S_{aq} T_{aq}}{\pi \cdot t}} \qquad (3.4)$$

In these equations, r is the distance between pumping well and piezometer, Q_p is well discharge, T_{aq} is aquifer transmissivity, R is the radius of the pumping cone, t is time, S_{aq} is aquifer storage coefficient, q* is discharge per unit length and s_p is well drawdown.

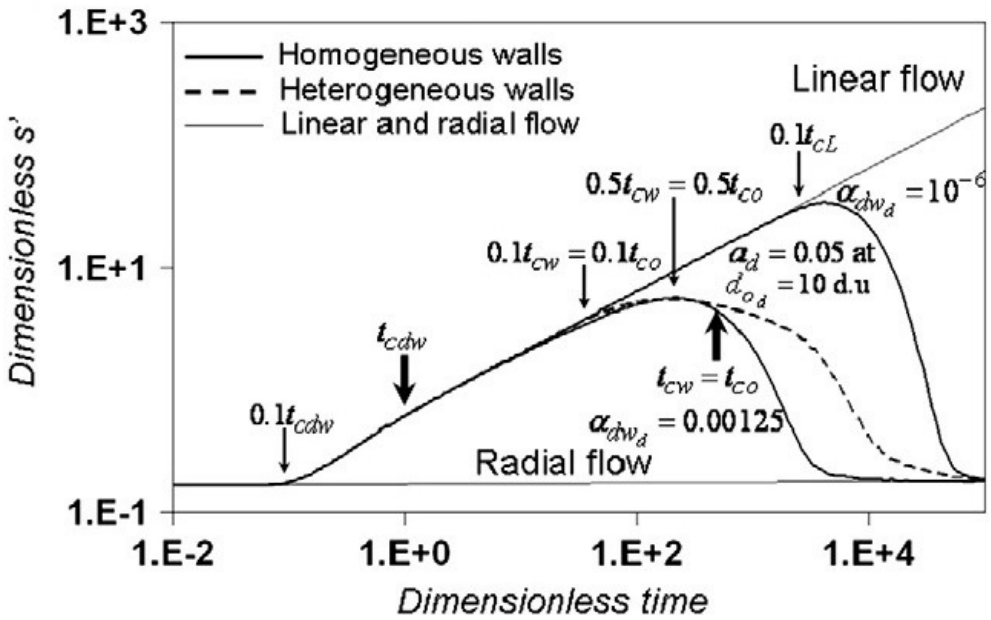

Figure 3.4. Diagnostic plot plotted with theoretical radial flow and linear flow evolution (Pujades et al., 2012).

Figure 3.4 indicates the transition from radial to linear flow in early stages and the subsequent transition from linear flow to radial flow in later stages, as was schematized in Figure 3.3. It distinguishes between homogeneous diaphragm walls and heterogeneous diaphragm walls. Homogeneous walls are walls without openings or walls with uniformly sized openings that are uniformly distributed along the walls. Heterogeneous walls have some randomly distributed openings with varying size.

A main observation that can be read from Figure 3.4 is the time (d.u.) when the linear flow changes to radial flow, i.e. the time when a substantial volume of water is leaking through the diaphragm wall. This occurs at the time when the diagnostic plot has reached its maximum value. From Figure 3.4 it can be read that this time is $0.5t_{cw}$. Pujades et al. (2012) use the following expression for t_{cw}:

$$t_{cw} = \frac{S_{aq}(1/\lambda)^2}{T_{aq}} \qquad (3.5)$$

In this equation, $1/\lambda$ [L] is a typical value for the characteristic distance from the pumping well where the aquifer is influenced by its pumping.

From λ, the value for the leakage factor of the diaphragm wall (α_{dw} [L/T]) at locations in the order of magnitude $1/\lambda$ from the pumping well can be calculated (Pujades et al., 2012). They give a definition for this leakage factor which makes sense when the diaphragm walls are homogeneous. An indication is given on how conclusions about homogeneity can be drawn from the shape of the diagnostic plot (Figure 3.4): the diagnostic plot for a heterogeneous diaphragm wall decreases more gradually over time after $0.5t_{cw}$. Pujades et al. (2012) define the inverse of the characteristic distance as

$$\lambda = \sqrt{\frac{2\alpha_{dw}}{T_{aq} \cdot d_{dw}}} \qquad (3.6)$$

From Equation (3.6) it follows that

$$\alpha_{dw} = \frac{\lambda^2 \cdot T_{aq} \cdot d_{dw}}{2} \qquad (3.7)$$

This leakage factor is a weighted average value for the large water retaining parts of the walls and the small openings in between.

From Equation (3.7), the hydraulic resistance (c [T]) of the diaphragm wall can be calculated (Pujades, 2012):

$$c = \frac{d_{dw}}{\alpha_{dw}} \qquad (3.8)$$

3.4. Analytical method for calculating leakage discharge

Bruggeman et al. (1985) have derived an analytical method to calculate the leakage discharge (Q [L^3/T]) through a joint between parts of a diaphragm wall. The relationship between leakage discharge and the properties of both the diaphragm wall and the aquifer is given by Equation (3.9). This equation is derived in Appendix 1.

$$Q = \frac{K \cdot S \cdot H}{d + \frac{F(\alpha)\sqrt{S}}{\pi}} \qquad (3.9)$$

In Equation (3.9), K is hydraulic conductivity, S is surface area of the joint, H is head difference over the wall, d is diaphragm wall thickness, α is the ratio of joint length to joint width and F(α) is some dimensionless function of α, defined in Appendix 1.

3.5. Spatial interpolation by ordinary kriging

Ordinary kriging is a spatial interpolation procedure in which the parameter value at a non-measured location is predicted by the measurement values of some locations in the surrounding area. The procedure results in an unbiased, optimal, linear prediction for the parameter value at the non-measured location (Bierkens et al., 2011; Kurtulus et al., 2011). Besides this prediction for the parameter value, results of ordinary kriging can be used to calculate the variance of the prediction error (Bierkens et al., 2011). Ordinary kriging requires that the parameter values over the area considered are realizations of a wide sense stationary random function with a constant mean, which may be unknown (Bierkens et al., 2011).

The relative contribution of the measurement value at some observed location to the parameter prediction at a non-measured location is calculated by the semivariogram. The semivariogram is a mathematical function that attributes a relative weight to a measurement, dependent on the distance between the measured location and the location where the parameter value is predicted. The semivariogram also has some parameters that depend on the characteristics of the random function that underlies the realizations. These parameters are the variance of the random function and its major range. The major range is

a scale for the length over which the values of two data points are still correlated (Bierkens et al., 2011). In practice, the semivariogram parameters are often estimated from the dataset (Pardo-Igúzquiza et al., 2012).

Some typical, often used models for the semivariogram are the spherical model, the Gaussian model and the exponential model (Bierkens et al., 2011). The expression for the semivariogram in an exponential model is given by Equation (3.10) (Bierkens et al., 2011):

$$\gamma_Z(h) = \sigma_Z^2 \cdot (1 - \exp(-h/a)) \qquad (3.10)$$

In this equation, Z is the parameter that is to be predicted (e.g. hydraulic head), σ_Z^2 is the variance of Z and *a* is the major range of Z. This semivariogram is a function of h, which is the distance between two data points. The variance of Z may be divided into two variances, each of which is operating at a different scale. One part, that is usually a small fraction of σ_Z^2, is called the nugget variance. The remaining, larger part is called the partial sill variance (Pardo-Igúzquiza et al., 2012). The nugget variance indicates the variance on very small scales by measurement errors or by parameter variations at a scale that is smaller than the distance between the mutually closest measurement locations. The partial sill variance accounts for the larger scale variations (Pardo-Igúzquiza et al., 2012).

3.6. Actively testing a water resistant screen by geoelectrical measurements

The German company Texplor GmbH has set up and patented a geoelectrical measurement method that, among other purposes, can test the watertightness of water resistant screens like sheet pilings and diaphragm walls at underground building sites. Usually, only a part of a water resistant screen is tested during such a measurement. The measurements are performed in case of a leakage in the water resistant screen that cannot be precisely located. The location of such a leakage is typically below the excavation level. The presence of a leakage can for example be observed by an excessive discharge rate required to maintain a reduced groundwater level or by an artesian well that appears inside the building site. Leakages in a diaphragm wall usually occur at the transitions between the elements of which it consists (see Section 3.2). Sheet pilings consist of knurled, steel elements that are typically 60 centimeters wide. These elements are interconnected by locks at their edges (see Figure 3.5). Leakages in sheet pilings are usually caused by water flowing through locks that are badly connected due to careless construction or due to displacement of the sheet piling during excavation of the building site.

The geoelectrical method is based on the physical property that electrical currents flow by the path that has the least electrical resistance (Heinz et al., 2011). Two electrical poles are used for testing a screen: one source pole is installed in a piezometer outside but near the building site concerned, and the other, oppositely charged or uncharged pole is located inside the building site. This second pole (the 'antipole') is located opposite the part of the screen that is tested and relatively distant from it. When a leakage in a water resistant screen is present, the two electrical poles are directly connected via the groundwater. As a consequence, the electric potential of the groundwater inside the building site near the location of the leakage is adjusted by the potential of the source pole outside. The geoelectrical method therefore aims at observing one or more locations on the inside of the wall where an anomalous electrical groundwater potential is present. The measurement of the groundwater potential is done by unpolarized measuring sensors which are installed in a dense grid. When testing a sheet piling, a sensor is located at each lock connecting two elements. Also, some sensors are placed in a grid that is somewhat more distant from the sheet piling. These sensors typically have a mutual distance of a few meters.

Figure 3.5. Sheet pilings.

The arrangement of the measurement equipment is shown in Figure 3.6. For every eight sensors, one data acquisition unit (the yellow devices in Figure 3.6) is required. Also one or more reference sensors are connected to a data acquisition unit. These reference sensors are placed at a distant location from the measurement area and are used as a control measurement to validate the results in the measurement area. All the data acquisition units used in the measurement procedure are interconnected by cables like the purple ones shown in Figure 3.6. The interconnected data acquisition units, together with the source pole, antipole and a laptop are connected to a power supply device, which is the gray device in Figure 3.6. This device obtains its power from an ordinary wall socket.

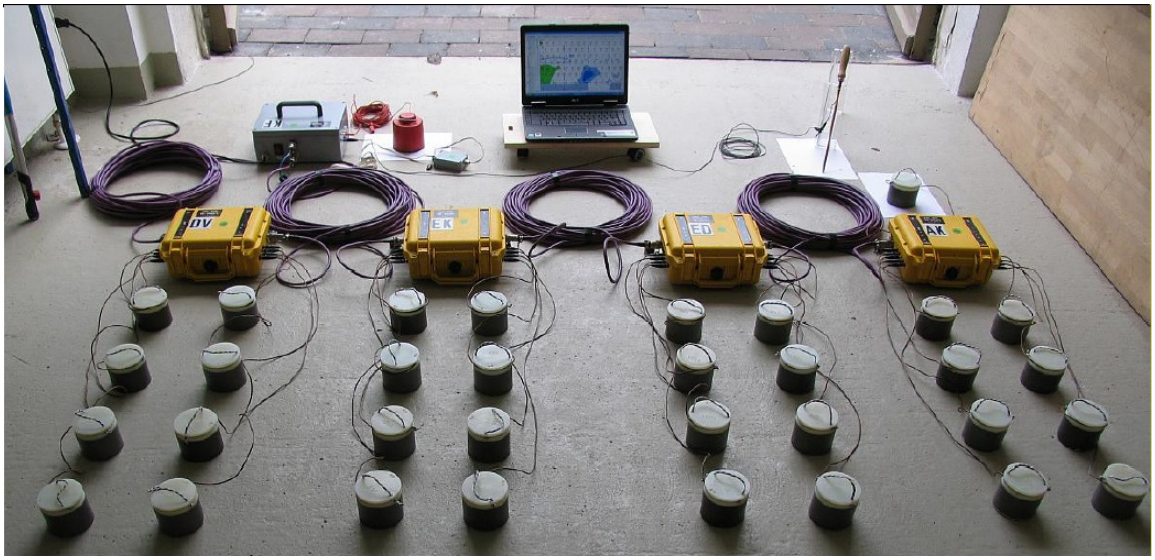

Figure 3.6. Geoelectrical measurement equipment (Heinz et al., 2011).

The actual measurement is done semi-automatically by the power supply device. This device only requires the manual input of the desired values for the voltages applied to the source pole. Typically, a small series of about five values for this voltage is applied in order to compare multiple results from the data analysis described three paragraphs ahead and in Chapter 7. This series of measurements always starts with a self potential measurement, which implies that no voltage is applied to the source pole. By this measurement, the self potential of the groundwater is measured. Its results are used to offset natural potential anomalies: the self potential measurement values are subtracted from the results from subsequent measurements, so those results only show the net effect of the voltage applied to the source pole.

After measuring the self potential, measurements with increasing voltages applied to the source pole are performed, according to the series that was manually given as input. For each value for voltage, typically ten measurements are performed, with a typical time interval in the order of ten seconds. So each of the voltages in the measurement series is continuously applied for a couple of minutes. The first few measurements for each value for voltage may show a stepwise increase in potential measured by the sensors because the groundwater potential has not yet fully adjusted to the increased voltage. But the later measurements should show mutually comparable results, and one of these measurement results is used in subsequent data analysis.

When a steel sheet piling is tested for leakages, the voltage applied to the source pole should not exceed a value in the order of 100 millivolts: the electrical current conducted by the sheet piling itself becomes increasingly important with increasing voltages and may eventually make the current conducted by the leaking groundwater negligible and invisible. When a diaphragm wall is tested, higher values for voltage are possible or even necessary because its elements usually have a thickness of more than a meter. Therefore, leaking joints between elements of a diaphragm wall have a higher electrical resistance than a leaking lock in a sheet piling.

The measurement results from all sensors are spatially interpolated by a kriging procedure. This interpolation is done automatically by a software package that is developed for this purpose. From the kriging procedure, a map with equipotential lines results. When a leakage is present at a lock between parts of a sheet piling, an anomaly in the electrical groundwater potential is generally not only measured by the sensor placed at this specific lock, but also by sensors at adjacent locks and by sensors that are more distant from the sheet piling. An anomalous potential measured by only one sensor at a specific lock does not necessarily imply that this lock is leaking, because this anomaly may be caused by local disturbing factors like metal parts or a small drainage system. A leakage is therefore identified from the contours on the ‘equipotential map’ and not from the individual measurement results. The absolute potential values of the equipotential lines on the map are not used for interpreting the results, but instead it is the pattern of equipotential lines on the map that contains the relevant information from which a conclusion can be drawn. The interpretation of a real equipotential map is discussed in a case study in Chapter 7.

4. ACTIVELY TESTING THE STATE OF THE DIAPHRAGM WALL OF VIJZELGRACHT STATION

4.1. Method

The theoretical procedure by Pujades et al. (2012), described in Section 3.3, is applied to a real pumping test at Vijzelgracht Station in order to test the state of a part of its diaphragm wall. The pumping test of which the data are used in this research has been carried out on June 29th 2009 from 8am to 12am. The discharge rate during this pumping test was roughly constant, and only one pumping well has been used. Figure 4.1 shows the evolution of discharge rate over time during this pumping test.

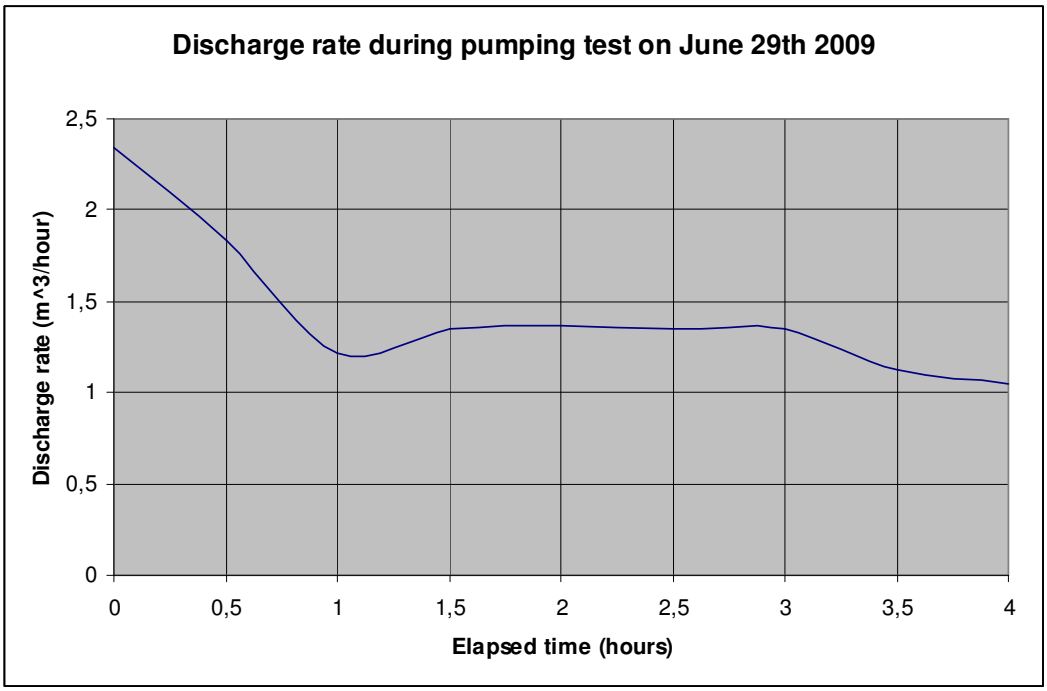

Figure 4.1. Evolution of discharge rate over time.

The head measurements of one piezometer located closest to the pumping well, at a distance of r=8.5 meter, are used in this analysis. Figure 4.2 shows the location of the pumping well (BV55) and piezometer (PBV60). The location of the pumping test is about 40 meters south from the middle of the building site, which has a total length of 254 meters.

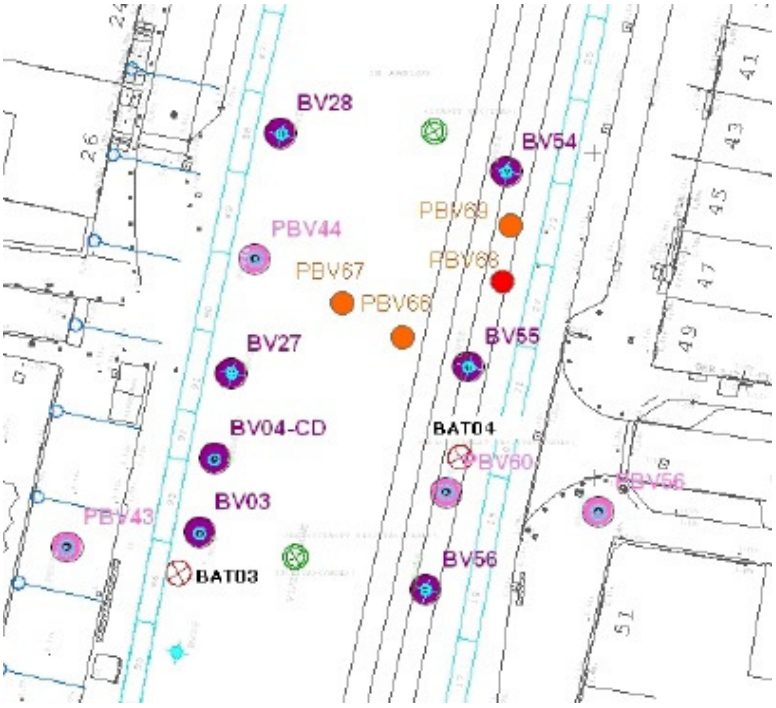

Figure 4.2. Location of pumping well (BV55) and piezometer (PBV60) (Duineveld, 2009). Scale indication: the distance between the two diaphragm walls (indicated by the light blue color) is d_{dw}=19 meter.

The pumping test has taken place in the 'tussenzandlaag' which is an aquifer consisting of both clay and sand, located between NAP-40 meter and NAP-41.5 meter at the location of Vijzelgracht Station. It has a low transmissivity of T_{aq}=0.4 m^2/day. The evolution of gross drawdown measured during the pumping test is shown in Figure 4.3. Heads were measured every two minutes over a period of four hours.

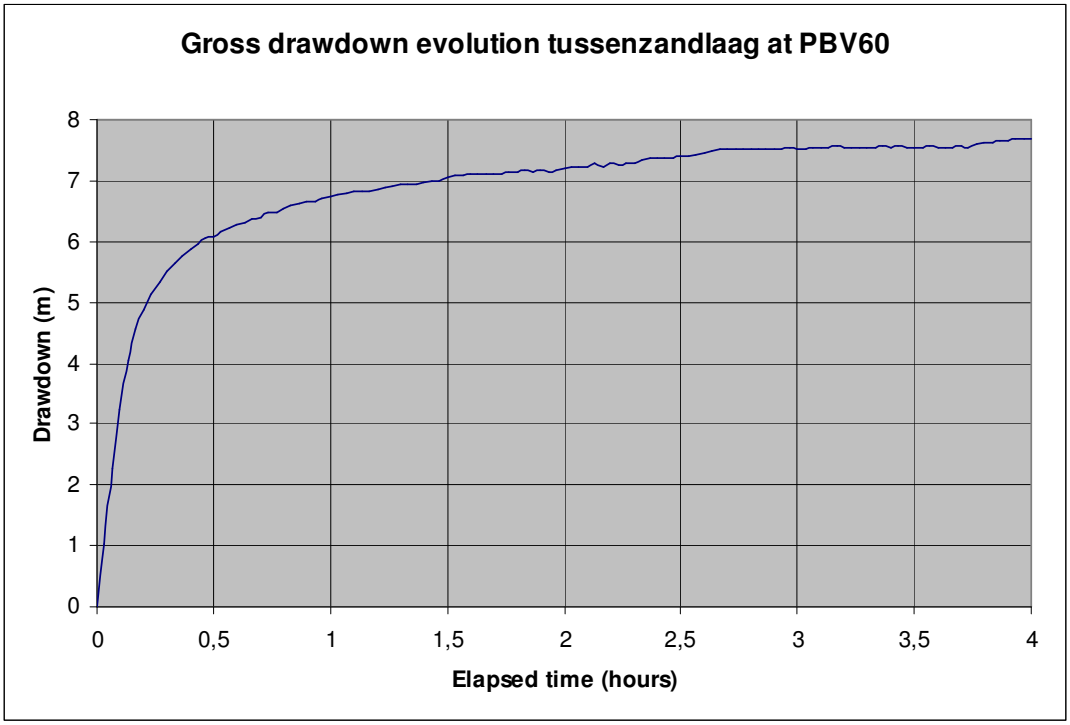

Figure 4.3. Gross drawdown evolution in piezometer PBV60.

The values for the diagnostic plot are calculated by discretizing Equation (3.1) and using dimensionless values for s and t:

$$s'(t_i) = \frac{s(t_i) - s(t_{i-1})}{\ln(t_i) - \ln(t_{i-1})} \qquad (4.1)$$

Equations (3.2) and (3.3) are used for the calculation of theoretical radial flow. Equation (3.4) is modified to Equation (4.2), which gives the evolution of hydraulic head for linear flow. Equation (4.2) is derived in Appendix 2.

$$h(r,t) = -s_p \sqrt{\frac{T_{aq} \cdot t}{S_{aq} \cdot \pi \cdot r^2}} + h(r, t=0) \qquad (4.2)$$

The definitions for dimensionless variables and their values used for this case study are shown in Table 4.1. The definitions are adopted from Pujades et al. (2012).

Type of variable	Characteristic variable	Equation	Value
Transmissivity	Aquifer transmissivity	$T_c=T_{aq}$	0.4 m^2/day
Storage coefficient	Aquifer storage coefficient	$S_c=S_{aq}$	0.0002
Length	Distance between diaphragm walls	$d_c=d_{dw}$	19 m
Discharge	Pumping well discharge	$Q_c=Q_p$	31.2 m^3/day
Drawdown	Well drawdown	$s_c=Q_p/T_{aq}$	78 m
Time	Pumping time	$t_c=S_{aq}*d_{dw}^2/T_{aq}$	0.1805 days
Leakage factor	Diaphragm walls leakage factor	$\alpha_c=T_{aq}/d_{dw}$	0.021 m/day

Table 4.1. Characteristic variables and values.

4.2. Results

The diagnostic plot for the pumping test on June 29th 2009 together with the theoretical results for radial and linear flow is shown in Figure 4.4.

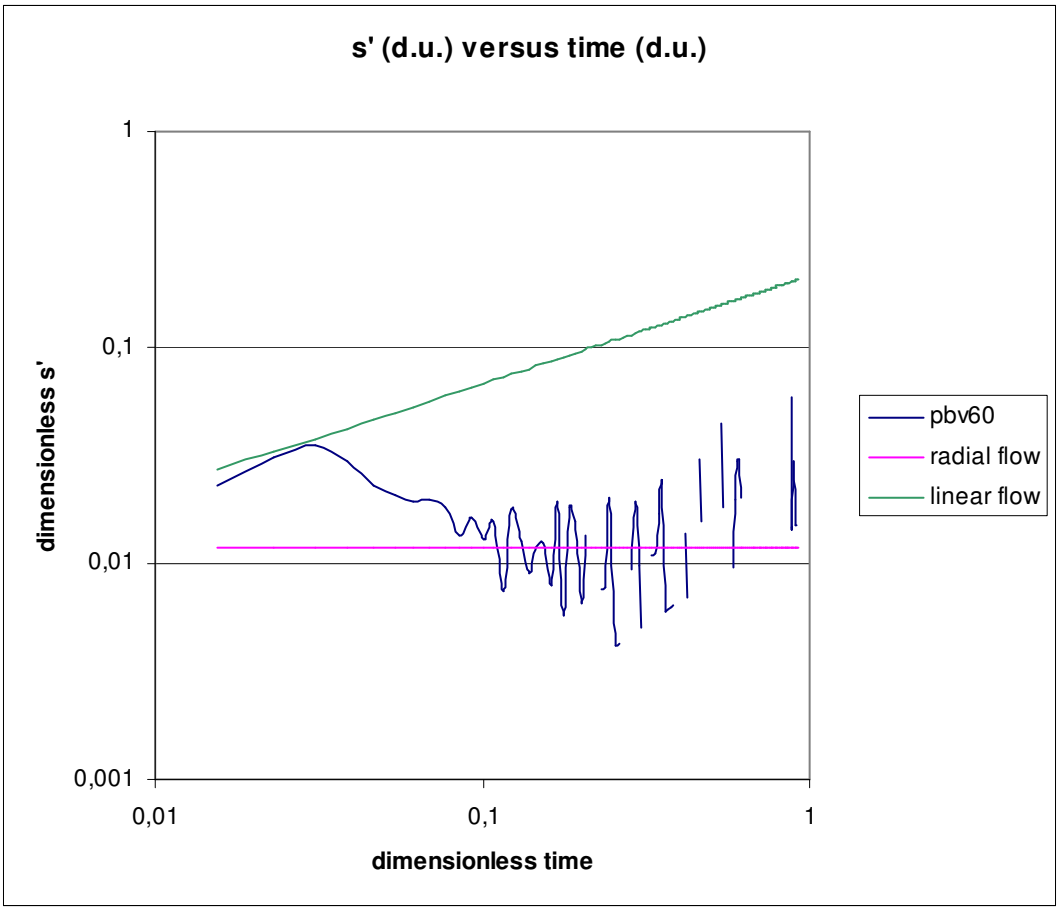

Figure 4.4. Diagnostic plot and theoretical radial and linear flow at piezometer PBV60.

The diagnostic plot in Figure 4.4 does not indicate radial flow at the very early stages of the pumping test, but it does indicate the transition from linear to radial flow. When imagining a trend line through the diagnostic plot, it approaches the line indicating radial flow after about t=0.1 (d.u.).

Some results from the diagnostic plot from t=0.1 (d.u.) can be observed. The limitations of these observations are explained in the discussion section (Section 4.3).

1. The diagnostic plot increasingly oscillates over time;
2. An imaginary trend line fitting the diagnostic plot increases at later times;
3. There are some discontinuities in the diagnostic plot.

The time when the diagnostic plot starts to decrease from its maximum, and is therefore leaving linear flow behavior, is read from the dataset used to draw Figure 4.4. From this dataset it is read that the maximum of the diagnostic plot is reached at t=0.031 (d.u.). According to Figure 3.4, this maximum is reached at $t=0.5t_{cw}$ (d.u.). Therefore, $t_{cw}=0.062$ (d.u.) and the non-dimensionless value (using Table 4.1) is therefore given by $t_{cw}=0.062*0.1805=0.0112$ days. Using Equation (3.5), λ^2 can be calculated:

$$\lambda^2 = \frac{S_{aq}}{T_{aq} \cdot t_{cw}} = \frac{0.0002}{0.4 \cdot 0.0112} = 0.0446 m^{-2} \qquad (4.3)$$

From Equation (4.3) it follows that 1/λ=4.7 meter. This is the result for the characteristic distance from the pumping well where the aquifer is influenced by its pumping.

Another result that can be obtained from λ is the value for the leakage factor of the diaphragm wall (α_{dw}) at locations in the order of magnitude 1/λ from the pumping well. Using Equation (3.7), the leakage factor is

$$\alpha_{dw} = \frac{\lambda^2 \cdot T_{aq} \cdot d_{dw}}{2} = \frac{0.0446 \cdot 0.4 \cdot 19}{2} = 0.17 m/day \qquad (4.4)$$

Finally, the hydraulic resistance of the diaphragm wall at locations in the order of magnitude 1/λ from the pumping well can be calculated using Equation (3.8):

$$c = \frac{d_{dw}}{\alpha_{dw}} = \frac{19}{0.17} = 112\ days \qquad (4.5)$$

4.3. Discussion

For the theoretical approach by Pujades et al. (2012), it is required that either the discharge rate from the pumping well or the head in the pumping well is fixed. Also, only one discharge well may be used. Though the first of these conditions is not satisfied during any pumping test at Vijzelgracht Station, the pumping test in the 'tussenzandlaag' of June 29th 2009 was assumed useful for this analysis. This is the most suitable pumping test among only a few ones available because the pumping rate was roughly constant during the test (see Figure 4.1), though it was above average in the early stage. Also, only one pumping well has been used.

Leakages in the 'tussenzandlaag' were expected in advance since there are no 'stop-ends' present between the elements of the diaphragm wall at this depth. Because it turned out to be impossible to construct these stop-ends up to this depth, openings up to a few centimeters width are expected between the elements of the diaphragm wall (Bhageloe, 2004).

The curve of gross drawdown evolution in piezometer PBV60 (Figure 4.3) is not increasing continuously, which can be explained by the occurrence of measurement errors, but also by small scale variations in environmental factors like atmospheric pressure. Since data on these variations are unavailable, only data on gross drawdown measurements can be used.

The original results for radial and linear flow have been multiplied by a factor 0.15 and 0.17 respectively in order to gain the results shown in Figure 4.4, where the diagnostic plot is nicely distributed in between. This is not assumed to undermine the conclusions for the following reasons:

1. The procedure to make the variables dimensionless uses some characteristic values (Table 4.1), which may not be perfectly determined;
2. The diagnostic plot is especially used to draw conclusions on its behavior at a specific time. This time is not influenced by a factor multiplication;
3. The correction factors do not differ from 1 by several orders of magnitude, and the correction factors for radial and linear flow are approximately equal.

The diagnostic plot in Figure 4.4 does not indicate radial flow at the very early stages of the pumping test. Two possible explanations are:

1. The pumping well is located at only about 2.5 meters from the diaphragm wall so that the cone of depression of the early radial flow is changed to linear flow very soon;
2. The flow behavior of the first four minutes is not shown in Figure 4.4. This is due to the fact that the logarithmic of time is taken in Equation (4.1), but one cannot take the logarithm of zero.

Some results stated below Figure 4.4 require some discussion:

1. The diagnostic plot increasingly oscillates over time. This can be explained by the high sensitivity of the diagnostic plot for measurement errors or inaccuracy of the measurement equipment. It can also be analytically explained by Equation (3.1): $s' = t(\partial s/\partial t)$. Since s' is some derivative multiplied by t, it can easily be understood that measurement errors are increasingly amplified at later times causing increasing oscillating behavior (Renard et al., 2008). Another example of a disturbing factor is the variation of well drawdown during the pumping test;
2. Also the trend line itself is sensitive to inaccuracies at later times for the same reason as given above, causing the imaginary trend line to ascend after some time;
3. There are some discontinuities in the diagnostic plot. The reason is that drawdown is not continuously increasing over time, as could be seen in Figure 4.3. The data points with lower drawdown compared to an earlier measurement are therefore manually excluded from the dataset, causing these discontinuities.

Pujades et al. (2012) state that conclusions on homogeneity can be drawn from the shape of the diagnostic plot (Figure 3.3). But since the distinction between a diagnostic plot indicating a homogeneous diaphragm wall and one indicating a heterogeneous diaphragm wall is not easily made, especially from the noisy signal in Figure 4.4, no decisive conclusion about homogeneity can be drawn from it. The calculation of the diaphragm wall leakage factor (α_{dw}), and therefore the calculation of its hydraulic resistance (c), theoretically only makes sense for homogeneous diaphragm walls, so conclusions from its result should be drawn with cautiousness.

The hydraulic resistance of the diaphragm wall at locations in the order of magnitude $1/\lambda$ (4.7 meter) from the pumping well was found to be 112 days (Equation (4.5)). This value is lower than the value of 300 days that was found at the level of the 'tussenzandlaag' after a model optimization in Modflow (Salet, 2010). The latter value was found for the whole diaphragm wall except for the end faces. The difference in these values for hydraulic resistance may be caused by the imperfect conditions under which the data used in this chapter were obtained. It may also be caused by variations in hydraulic resistance over the diaphragm wall due to varying conditions under which different parts of it were constructed.

The analytical approach by Pujades et al. (2012) is the first and only study which deals with the specific topic of testing the state of a diaphragm wall framing a linear building site (Pujades et al., 2012). No other analytical methods have been developed yet, so no competitive analysis on an active test of the state of the diaphragm walls of Vijzelgracht Station was done.

4.4. Conclusions

Research question (1): what method can actively test the state of the diaphragm wall of Vijzelgracht Station using piezometer data?

Answer: the approach by Pujades et al. (2012) is the only analytical method available to interpret the results of an actively tested diaphragm wall of a linear excavation site. The analytical method by Pujades et al. (2012) is not useful to test the state of the diaphragm wall of Vijzelgracht Station in retrospective.

The arguments for this conclusion are:

1. The number of (useful) pumping tests at Vijzelgracht Station is much too low for testing the state of large parts of its diaphragm walls;
2. The characteristic length ($1/\lambda$), which indicates what piece of the wall is tested, is quite small in this case study. One would therefore need many pumping tests to cover the whole diaphragm wall, but these data are unavailable;
3. This analytical method only draws conclusions about the state of the wall at a specific depth, which is the 'tussenzandlaag' in the case study considered. Either one would have to assume that the properties of the diaphragm wall is constant with depth, which is not likely, for example because the stop-ends are not present up to the depth of the tussenzandlaag, or one would have to do pumping tests in all three aquifers present at Vijzelgracht Station;
4. The method is very sensitive to the data available, as could be read from the noisy signal in Figure 4.4. For example the assumption that well discharge is constant over time is hardly seen in pumping tests. Also, there is only a few pumping tests available during which only one pumping well was operating. This is required in order to attribute the drawdown measured in a specific piezometer to that specific pumping well.

The analytical approach by Pujades et al. (2012) could be useful for testing the state of a diaphragm wall when pumping tests have been set up with the specific goal to use the generated data for analysis as presented in the case study in this chapter. This implies that, for example, the discharge rate should really be kept constant over time. Also, a sufficient number of pumping tests distributed along the whole diaphragm wall should be done in order to draw conclusions about the whole wall. However, doing sufficient pumping tests at Vijzelgracht Station, and at any building site in general, is costly and laborious.

4.5. Recommendations

The method of actively testing the state of a diaphragm wall described in this chapter was concluded to be not usable for Vijzelgracht Station on the scale of the whole station. Investing in a passive rather than an active testing method may be more advantageous. An adequate passive testing method can timely localize a leakage occurring. A passive testing method by piezometer measurements is discussed in the next two chapters.

5. OPTIMIZING PIEZOMETER CONFIGURATION FOR LOCALIZING A THEORETICAL LEAK IN A DIAPHRAGM WALL

5.1. Method

5.1.1. Rationale behind the method

A leakage in a diaphragm wall causes a head drawdown outside the building site, which is measured by piezometers. To test the suitability of a specific piezometer configuration for localizing a leak, a Modflow model is made in which a diaphragm wall is placed into an imaginary, layered soil system. In this system, a leakage in the wall is simulated at a known position. A large number of piezometers are put outside the diaphragm wall, which record the head drawdown over time. Piezometer data from Modflow at a specific time after the occurrence of the leakage are exported to ArcGIS. These piezometer data are used in ArcGIS to obtain the head values over the whole area outside the diaphragm walls that is framed by the farthest piezometers. This interpolation is done by ordinary kriging. From all interpolation data, the data on the line that is directly adjacent to the diaphragm wall are exported to Excel. These data points are plotted versus their corresponding position along the wall. The position along the diaphragm wall where the curve has its minimum is interpreted as the location of the leakage. This location is compared to the known location of the leakage that was set in Modflow. The closer the location of the leakage read from the curve in Excel to the known value that was set in Modflow, the better the corresponding piezometer configuration. This interpolation procedure is repeated for many piezometer configurations, so every time a different subset of the head data exported from Modflow is used. To summarize, specific piezometer configurations are tested on their ability to localize a leakage in a diaphragm wall.

In this chapter, 6 scenarios for the aquifer properties at the level of the leaking diaphragm wall are tested. These scenarios are specified in the next section. In each scenario, different values for the following aquifer variables are combined:

1. Conductivity (3 values);
2. Layer thickness (3 values);
3. Leakage discharge (6 values);
4. Time after occurrence of the leakage at which the analysis is applied (4 values).

Not all possible combinations of these values for parameters are tested; only 6 sensible combinations (6 scenarios) are applied.

5.1.2. Simulating a leakage in Modflow

In Modflow, a building site framed by diaphragm walls is located in a model area of 500 by 500 meters. The dimensions of the building site are 100 by 100 meters, and it is located in the middle of the model area. The model consists of four layers. The properties of these layers are given in Table 5.1. The thickness and conductivity of layer 2, which is the layer in which a leakage is simulated, varies over different scenarios that are simulated. Its thickness and conductivity are specified at each specific scenario.

Layer	Property	Thickness (m)	Initial head (m)	Horizontal conducti-vity (m/day)	Vertical conducti-vity (m/day)	Specific storage (m^{-1})	Effective porosity (-)
1	aquitard	3	-0.5	0.005	0.005	0.0001	0.25
2	aquifer	varying*	-1	varying*	varying*	0.0001	0.25
3	aquitard	5	-1.2	0.005	0.005	0.0001	0.25

4	aquitard	5	-1.2	0.005	0.005	0.0001	0.25

*Table 5.1. Model properties. *Some properties of layer 2 are varying over different scenarios.*

The cells bordering the model area in layers 1 through 3 are assigned a constant head value. Layer 4 is wholly assigned a constant head value. All constant head values are the respective initial head values given in Table 5.1. The model cells inside the building site have dimensions of 1 by 1 meter. The model cells in the area of 300 by 300 meters centered in the model area (but excluding the building site) have dimensions of 2 by 2 meters. The outermost cells that are closer than 100 meter from the model borders have dimensions of 4 by 4 meters.

The diaphragm wall is modeled in layer 1 and 2. It is modeled by assigning both horizontal and vertical conductivity a value of 0.0005 m/day to cells at the location of the wall. Other cell properties of these cells are equal to the values for the respective layer in Table 5.1. The thickness of the diaphragm wall is 1 meter, but at the northern side it has a thickness of 2 meters. The leakage is simulated in the northern side of the wall. Therefore, a lot of piezometers are placed north of the building site. These piezometers measure the head in layer 2. A total number of 267 piezometers are placed, set in five rows of 53 with a mutual distance of 2 meter longitudinally along the diaphragm wall. The distances of these five rows from the diaphragm wall are 2, 4, 8, 12 and 16 meters respectively. Two additional piezometers are located at the line adjacent to the diaphragm wall: one is located 2 meters west from its borders while another is located 2 meters east from its borders. By doing so, ArcGIS will include the area directly adjacent to the diaphragm wall in the kriging procedure. The northern part of the diaphragm wall together with the locations of the piezometers is shown in Figure 5.1.

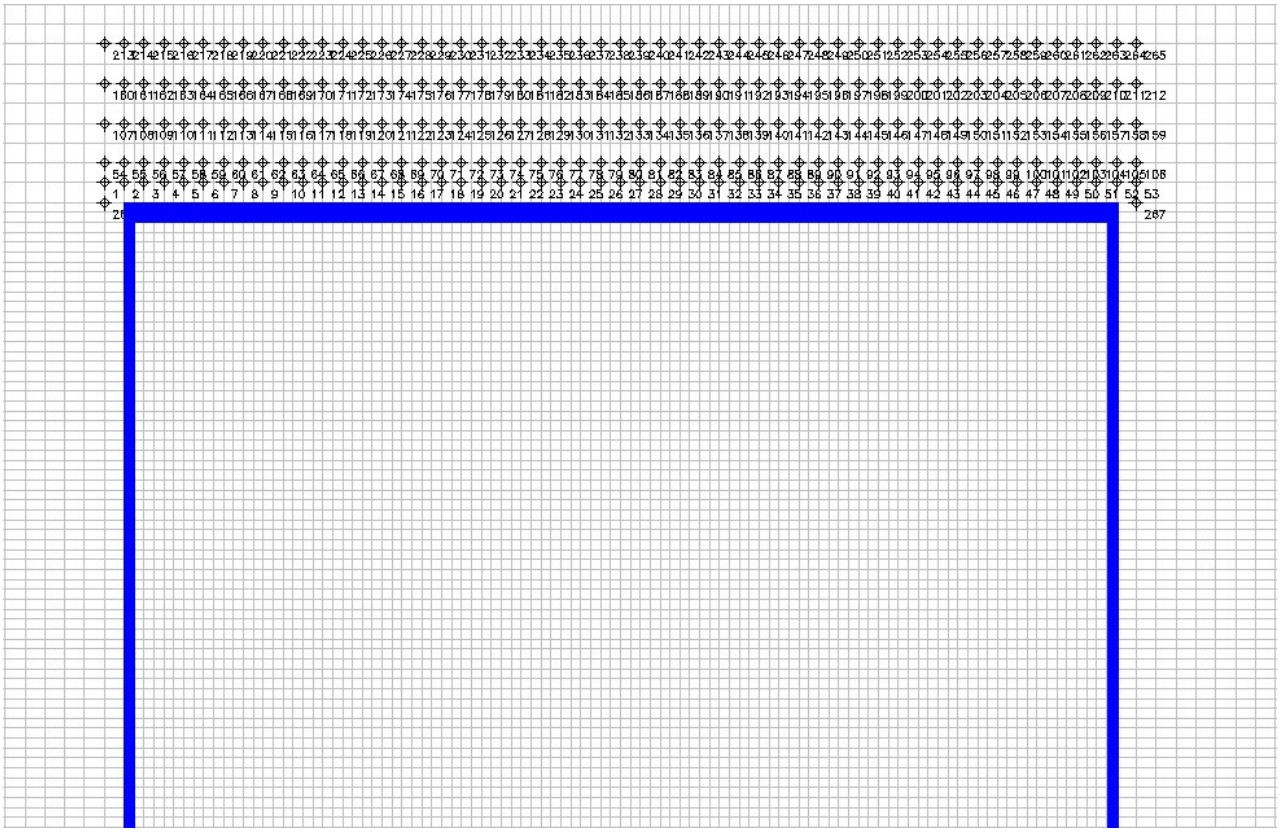

Figure 5.1. 267 piezometers are modeled at the northern part of the model area. Note for scale: the width of the building site is 100 meters.

The simulation type in Modflow is set to transient flow. Two time periods are used:

1. Period 1 has time length 1 day, divided into 4 time steps. Period 1 is used to obtain a steady-state head distribution prior to the occurrence of the leakage;
2. Period 2 has time length 2 days, divided into 48 time steps. The leakage is modeled to occur in period 2. The evolution of head over time can be read per hour by these settings.

A leakage is successively simulated in single cells in the northern part of the diaphragm wall. This leakage is modeled by putting a well in one cell of the diaphragm wall, bordering the area outside the building site. The leakage occurs in layer 2 during time period 2. This simulation is repeated for three different values for horizontal and vertical hydraulic conductivity in layer 2, two of which are 30 m/day and 1 m/day. These two values correspond to a coarse sand layer and a silty sand layer respectively. For the leakage occurring the coarse sand layer (K=30 m/day), three scenarios for leakage discharge are modeled. For the leakage occurring in the silty sand layer (K=1 m/day), two scenarios for leakage discharge are modeled (see Table 5.2). The thickness of layer 2 is changed when changing the leakage discharge: a relatively large leakage is modeled using a relatively thick aquifer and vice versa.

Besides the five scenarios for leakages in sand layers, also a leakage in a relatively pervious clay layer with K=0.03 m/day is modeled in one last scenario. The Modflow model used for this scenario has undergone some modifications with respect to the properties given above:

1. Layer 2 is divided into three layers: 2a, 2b and 2c, each of which has a thickness of 2 meters. The leakage is modeled in layer 2b, which has a horizontal and vertical conductivity of 0.03 m/day. Layers 2a and 2c both have a horizontal and vertical conductivity of 1 m/day. Other parameter values are equal to those in given in Table 5.1 for layer 2;
2. Piezometers are placed in layer 2b;
3. Time period 1 has time length 14 days, divided into 4 time steps. This extension is required for obtaining a steady-state head distribution prior to the occurrence of the leakage.

The values for conductivity are not taken to be exactly the value given in the paragraph above. Instead, the Field Generator in Modflow is used to generate some more realistic distribution for conductivity values around this average value. The standard deviation of the conductivity field is taken to be 10% of the average value. The correlation length of the conductivity field along both rows and columns is taken to be 0.05.

For each of the six scenarios, five separated locations (realizations) for the leakage are simulated. This implies that a total number of 5 (realizations) times 6 (scenarios) is 30 simulations are run in Modflow. Many possible piezometer configurations (18 per simulation) are tested for all these 30 simulations from Modflow.

Before applying a procedure for localizing a leakage in daily practice, one must be able to notice that this leakage is occurring anyway. This reasoning is applied in this theoretical research. Therefore, head data from the piezometers in Modflow are exported at a time at which one would be able to read from these data that a leakage is occurring anyway (but its location is still unknown). In this research, this means that a head gradient is observed in between some piezometers. The usefulness of a specific configuration in each realization is

not only judged by its ability to localize the leakage, but also by its ability to notice the leakage at all.

A realization of a specific piezometer configuration is considered as 'satisfactory' *for noticing the occurrence of a leakage* when a hydraulic head gradient of at least 0.0025 is observed between any two piezometers in this configuration. For scenario 6, in which a leakage occurs in a clay layer (K=0.03 m/day), this value for hydraulic gradient is taken to be 0.001. A specific piezometer configuration is considered as 'satisfactory' *for localizing a leakage* when the average error of 5 realizations is less than 1.5 meters. The 'error' is defined as the distance between the modeled (known) location of the leakage in Modflow and the location predicted by the kriging procedure.

The six scenarios that are modeled in Modflow are given in Table 5.2. This table states the (average) conductivity in layer 2, in which the leakage occurs. It also states the leakage discharge, the thickness of layer 2, the transmissivity (KD-value) and the time after the occurrence of the leakage at which the piezometer data are saved and exported from Modflow to ArcGIS. In the last five columns, the locations of the leakages for the five realizations of each scenario are given. These values are given in meters eastern from the northwestern part of the diaphragm wall.

Sc.	Conducti-vity layer 2 (m/d)	Dis-charge (m^3/d)	Thick-ness layer 2 (m)	KD-value (m^2/d)	Time (hrs)	Loc. 1 (m)	Loc. 2 (m)	Loc. 3 (m)	Loc. 4 (m)	Loc. 5 (m)
1	30	12	2	60	12	44.5	7.5	62.5	71.5	31.5
2	30	36	6	180	6	77.5	43.5	90.5	15.5	36.5
3	30	216	20	600	2	49.5	83.5	36.5	71.5	8.5
4	1	0.5	2	2	12	47.5	65.5	8.5	78.5	23.5
5	1	2	6	6	4	40.5	14.5	80.5	31.5	57.5
6	0.03	0.25	2*	0.06	12	60.5	11.5	18.5	78.5	43.5

*Table 5.2. Overview of the scenarios run in Modflow. *This is the thickness of layer 2b.*

5.1.3. Interpolation of head measurements by ordinary kriging in ArcGIS

A total number of 18 subsets of the piezometer measurement dataset that is exported by Modflow are used in ArcGIS for kriging. Each of these 18 subsets of piezometers corresponds to a specific piezometer configuration. An overview and description of these 18 configurations is given in Table 5.3. It also states the number of piezometers that are used in each configuration.

Configu-ration	Description of piezometer configuration	Number of piezometers
A	row at 2 meters from wall, mutual distance 4 meters	27
B	row at 2 meters from wall, mutual distance 8 meters	14
C	row at 2 meters from wall, mutual distance 12 meters	9
D	row at 4 meters from wall, mutual distance 4 meters	27
E	row at 4 meters from wall, mutual distance 8 meters	14
F	row at 4 meters from wall, mutual distance 12 meters	9
G	row at 8 meters from wall, mutual distance 4 meters	27
H	row at 8 meters from wall, mutual distance 8 meters	14
I	row at 8 meters from wall, mutual distance 12 meters	9
J	3 lines of 3 piezometers perpendicular to wall	9
K	3 lines of 5 piezometers perpendicular to wall	15

L	4 lines of 3 piezometers perpendicular to wall	12
M	4 lines of 5 piezometers perpendicular to wall	20
N	6 lines of 3 piezometers perpendicular to wall	18
O	6 lines of 5 piezometers perpendicular to wall	30
P	row at 12 meters from wall, mutual distance 4 meters	27
Q	row at 12 meters from wall, mutual distance 8 meters	14
R	row at 12 meters from wall, mutual distance 12 meters	9

Table 5.3. Description of 18 piezometer configurations.

These configurations are visualized in Figures 5.2 through 5.7. The letters indicate the corresponding configuration in Table 5.3. The blue line in the figures indicates the northern border of the diaphragm wall. The X indicates the location of the leakage in the first realization of scenario 1 in Table 5.3, which is 44.5 meters eastern.

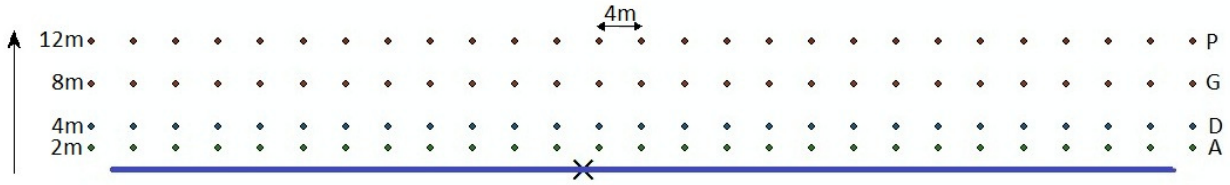

Figure 5.2. Configurations A, D, G and P.

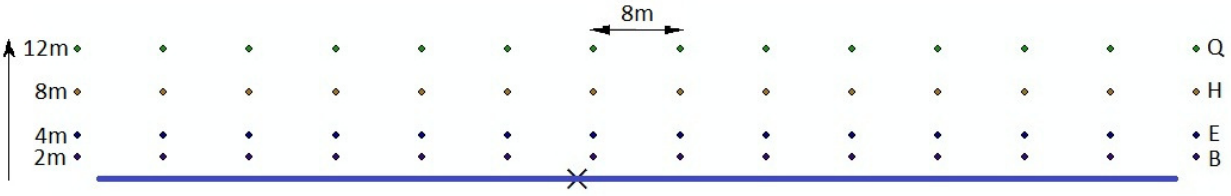

Figure 5.3. Configurations B, E, H and Q.

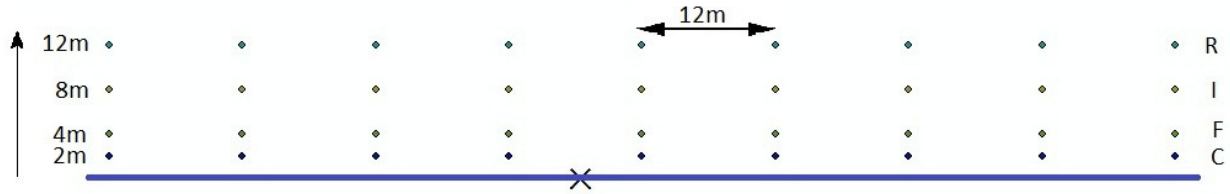

Figure 5.4. Configurations C, F, I and R.

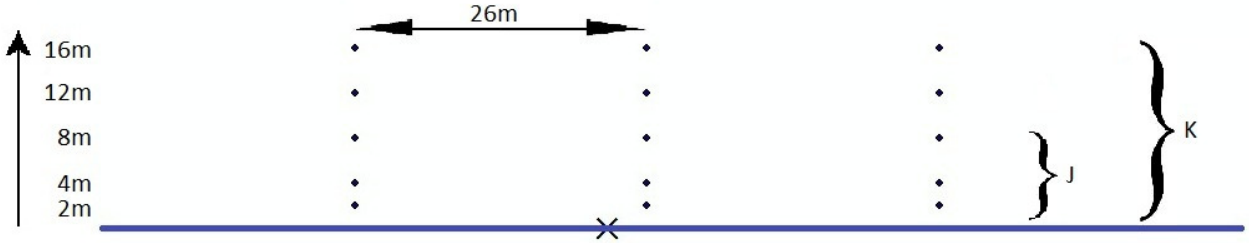

Figure 5.5. Configurations J and K correspond to rows of piezometers that are perpendicular to the diaphragm wall.

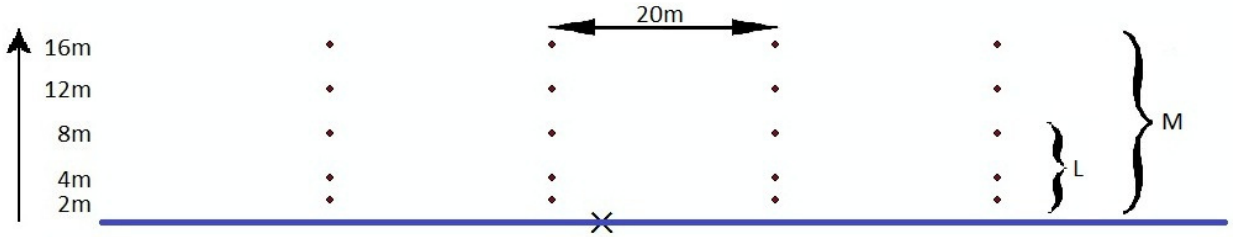

Figure 5.6. Configurations L and M correspond to rows of piezometers that are perpendicular to the diaphragm wall.

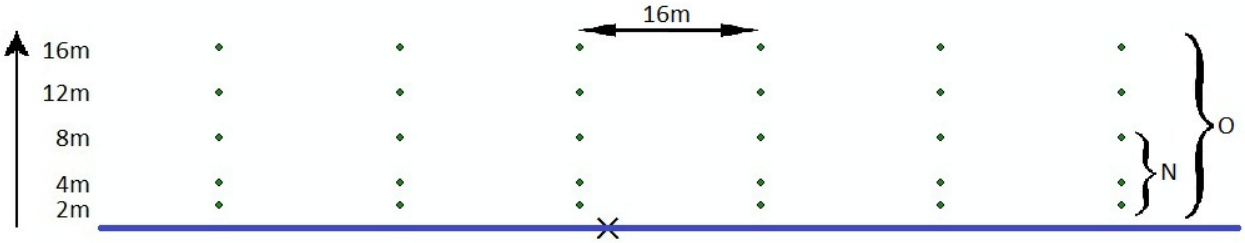

Figure 5.7. Configurations N and O correspond to rows of piezometers that are perpendicular to the diaphragm wall.

For all 5 realizations of all 6 scenarios in Table 5.3, the 18 piezometer configurations are imported into ArcGIS (configurations P, Q and R are not applied for scenario 6). In ArcGIS, ordinary kriging is performed on these configurations. An exponential semivariogram model is applied for the kriging procedure. The value for major range is taken to be 100 meters for all scenarios. This is the length of the diaphragm wall. The variance of the head measurements for each realization in Modflow is calculated in Excel. This variance is the sum of the partial sill variance and the nugget variance (Pardo-Igúzquiza, 2012). The nugget variance is taken to be about ten percent of the partial sill variance. The partial sill variance and nugget variance for the semivariogram model for the individual realizations of each scenario are given in Appendix 3.1.

A part of the kriging results of each configuration is exported to Excel, namely the interpolation results over the line that is directly adjacent to the diaphragm wall. These data points are plotted versus their corresponding position along the wall. The position along the diaphragm wall where the curve belonging to a specific configuration has its minimum is interpreted as the location of the leakage that is predicted by this specific configuration. This location is compared to the known location of the leakage that was set in Modflow.

The error belonging to a specific configuration is taken to be the difference between the location of the leakage that was set in Modflow and the location that is read from the curve that is obtained after the kriging procedure. The average error of 5 realizations is calculated in order to compensate for measurement errors and for dependency of the result on the location of the leakage that was set in Modflow.

5.2. Results

5.2.1. Results from the kriging procedure

An example of the visual result from the kriging procedure in ArcGIS is shown in Figure 5.8. This example shows the result for realization 1 of scenario 1 (see Table 5.2). In this specific example, the kriging result from configuration H (see Table 5.3) is shown, together with its corresponding piezometer configuration. The northern border of the diaphragm wall is indicated by the blue line. The location of the leakage set in Modflow is indicated by X.

A legend is also shown in Figure 5.8, but the absolute numerical results for head values along the wall are not useful. This is because the head drawdown along the wall is underestimated by the kriging procedure: the results from the kriging procedure indicate that the largest drawdown in the area is obtained at the location of the piezometer that has the largest drawdown. At any other location, the predicted drawdown is less than at the location of this piezometer. This is obviously not true in a real field situation, since the largest drawdown occurs directly adjacent to the diaphragm wall, at the location of the leakage. Therefore, the predicted head values that result from kriging are only used to predict the location of the leakage, which is at the minimum head value.

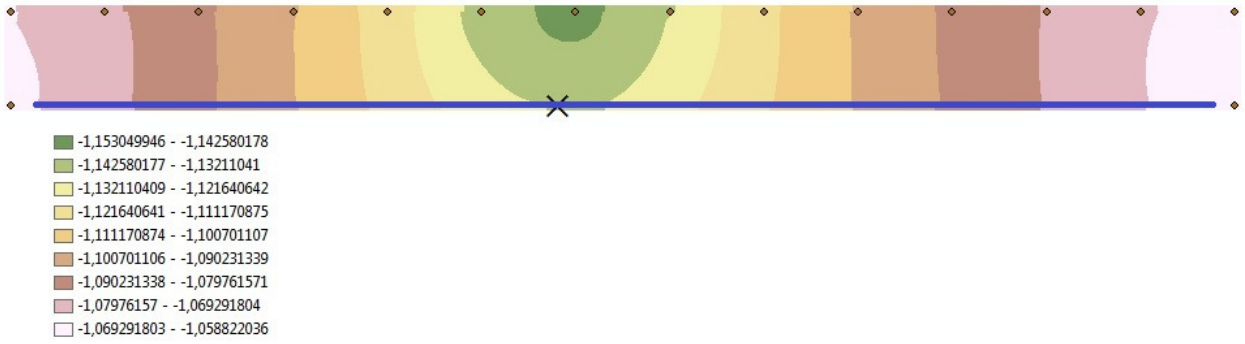

Figure 5.8. Example of a visual result from the kriging procedure. Head values are given in meters above NAP.

Figure 5.9 shows an example of a diagram that is drawn in Excel after importing the predicted head values from the kriging procedure. It shows the predicted head values at the line that is directly adjacent to the diaphragm wall. This specific diagram shows the results from the kriging procedure of piezometer configuration A through R of realization 1 of scenario 1. As discussed in the previous paragraph, the predicted head values underestimate the real drawdown along the diaphragm wall at the location of the leakage.

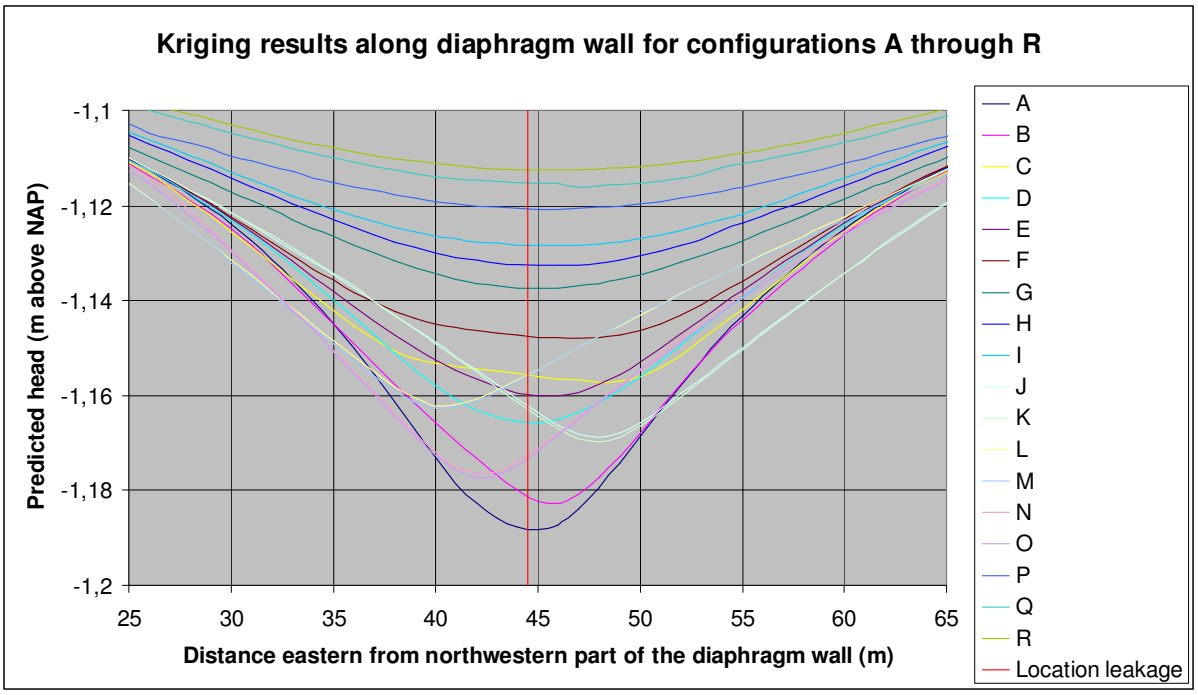

Figure 5.9. Example of the result from the kriging procedure. The red line indicates the location of the leakage that was set in Modflow.

The results for the average error and its standard deviation of each configuration in each realization for each of the six scenarios (see Tables 5.2 and 5.3) are given in separate tables. The results for scenarios 1 through 6 are given in Tables 5.4 through 5.9 respectively. Also the number of piezometers required for each configuration is given. The results for all individual errors of all realizations are given in Appendix 4.1. Appendix 4.1 also shows at which of these realizations the criterion for noticing the leakage fails due to an insufficient head gradient in the piezometer data underlying this specific realization.

Piezometer configuration	Number of piezometers	Average error of five realizations (m)	Standard deviation of five realizations (m)
A	27	**0.5**	0
B	14	**1.1**	0.55
C	9	**2.8**	1.48
D	27	**0.7**	0.45
E	14	**0.9**	0.55
F	9	**1.7**	1.30
G	27	**0.7**	0.45
H	14	**1.2**	0.67
I	9	**0.9**	0.55
J	9	**7.3**	4.21
K	15	**7.3**	4.21
L	12	**6.7**	3.49
M	20	**6.5**	3.39
N	18	**3.1**	0.89
O	30	**3.2**	0.97
P	27	**0.9**	0.74
Q	14	**1.8**	1.30
R	9	**2.3**	2.95

Table 5.4. Results for scenario 1.

Piezometer configuration	Number of piezometers	Average error of five realizations (m)	Standard deviation of five realizations (m)
A	27	**0.4**	0.22
B	14	**0.9**	0.55
C	9	**2.9**	1.34
D	27	**0.5**	0
E	14	**0.8**	0.67
F	9	**1.8**	1.20
G	27	**1.2**	0.97
H	14	**1.5**	0.94
I	9	**1.7**	1.15
J	9	**7.9**	4.68
K	15	**8.0**	4.74
L	12	**4.8**	2.99
M	20	**4.8**	2.99
N	18	**2.7**	1.64
O	30	**2.7**	1.64
P	27	**2.9**	3.19
Q	14	**2.4**	1.14
R	9	**1.8**	1.15

Table 5.5. Results for scenario 2.

Piezometer configuration	Number of piezometers	Average error of five realizations (m)	Standard deviation of five realizations (m)
A	27	**0.5**	0
B	14	**1.5**	0
C	9	**2.1**	1.52
D	27	**0.7**	0.45
E	14	**0.6**	0.55
F	9	**1.8**	1.57
G	27	**1.2**	0.76
H	14	**1.3**	0.76
I	9	**1.1**	0.89
J	9	**7.2**	4.89
K	15	**7.3**	4.97
L	12	**6.1**	2.88
M	20	**6.3**	2.95
N	18	**3.5**	1.46
O	30	**3.6**	1.52
P	27	**2.3**	2.93
Q	14	**1.5**	1.00
R	9	**1.7**	0.76

Table 5.6. Results for scenario 3.

Piezometer configuration	Number of piezometers	Average error of five realizations (m)	Standard deviation of five realizations (m)
A	27	**0.5**	0
B	14	**1.3**	0.45
C	9	**3.1**	0.89

D	27	**0.5**	0
E	14	**0.5**	0
F	9	**2.3**	0.84
G	27	**0.8**	0.67
H	14	**0.5**	0.35
I	9	**1.3**	0.27
J	9	**5.2**	4.69
K	15	**5.2**	4.69
L	12	**5.5**	3.39
M	20	**5.5**	3.39
N	18	**3.7**	1.64
O	30	**3.7**	1.64
P	27	**0.9**	0.96
Q	14	**1.3**	0.84
R	9	**2.3**	2.66

Table 5.7. Results for scenario 4.

Piezometer configuration	Number of piezometers	Average error of five realizations (m)	Standard deviation of five realizations (m)
A	27	**0.5**	0
B	14	**1.3**	0.45
C	9	**2.6**	1.24
D	27	**0.5**	0
E	14	**0.7**	0.57
F	9	**1.2**	0.84
G	27	**1.0**	1.41
H	14	**0.5**	0.35
I	9	**0.9**	0.42
J	9	**7.7**	0.84
K	15	**7.7**	0.84
L	12	**3.5**	3.46
M	20	**3.3**	3.11
N	18	**3.1**	2.07
O	30	**3.1**	2.07
P	27	**1.5**	1.84
Q	14	**0.9**	0.65
R	9	**1.0**	0.61

Table 5.8. Results for scenario 5.

Piezometer configuration	Number of piezometers	Average error of five realizations (m)	Standard deviation of five realizations (m)
A	27	**0.5**	0
B	14	**1.9**	0.89
C	9	**3.1**	1.08
D	27	**0.3**	0.27
E	14	**1.3**	0.57
F	9	**2.3**	0.76
G	27	**1.6**	1.85
H	14	**1.3**	1.04
I	9	**1.5**	1.41
J	9	**6.6**	3.36

K	15	**6.7**	3.51
L	12	**3.0**	3.00
M	20	**3.1**	3.21
N	18	**3.3**	2.17
O	30	**3.3**	2.17

Table 5.9. Results for scenario 6. Scenarios P through R were not applied in this scenario.

5.2.2. Piezometers parallel versus perpendicular to a diaphragm wall

With regard to placing a row of piezometers parallel versus perpendicular to a diaphragm wall, the results in Tables 5.4 through 5.9 indicate:

1. Placing a row of piezometers parallel to the diaphragm wall always results in a (much) more accurate predicted location of the leakage compared to placing these in some rows perpendicular to it. In only a few realizations the location predicted by a row parallel to the wall is as poor as is generally found by rows perpendicular to it. This result is even more interesting because hydrologists almost naturally prefer to place piezometers in rows perpendicular to a building site. The number of piezometers required for these rows are better placed in one single row parallel to a building site;
2. In view of localizing the leakage, the extension of such a row perpendicular to a diaphragm wall from 3 to 5 piezometers does not improve the result: the prediction of the location of the leakage remains poor;
3. When a leakage occurs closer than about 5 meters from a row of piezometers perpendicular to a diaphragm wall, the predicted location of this leakage is at the level of this row along the wall. When a leakage occurs more in between two rows of piezometers perpendicular to the wall, the predicted location is more compromised by piezometer data from these two rows, but it still tends towards the level of one of the rows.

5.2.3. Results on the coarse sand aquifer

Tables 5.4 through 5.6 and Tables A4.1 through A4.3 show the following results for the coarse sand aquifer (K=30 m/day):

1. Configuration E is the optimal configuration for the coarse sand aquifer. It has piezometers placed at 4 meters from the wall which have a mutual distance of 8 meters. This applies to all values for leakage discharge. Both the average error and the standard deviation of the individual realizations are small, and even their sum is below 1.5 meters. All realizations in this configuration satisfy the criterion for noticing the leakage from the piezometer data;
2. Given the distance of a row of piezometers from the diaphragm wall, the location of the leakage is usually best predicted by configurations in which these piezometers have a mutual distance of 4 meters. But this dense configuration is not required in order to satisfy the criterion for localizing a leakage;
3. Configuration I accurately predicts the location of a leakage in some of the realizations. It has piezometers placed at 8 meters from the wall which have a mutual distance of 12 meters. However, the average error fails the criterion for localizing a leakage in one of the three scenarios tested. Also the standard deviation of the individual realizations is high for two of the three scenarios. The criterion for noticing the leakage from the piezometer data fails in 25 percent of the realizations.

5.2.4. Results on the silty sand aquifer

Tables 5.7, 5.8, A4.4 and A4.5 show the following results for the silty sand aquifer (K=1 m/day):

1. Configurations E and H are the optimal configurations for the silty sand aquifer. These have piezometers at 4 or 8 meters from the wall respectively which have a mutual distance of 8 meters. This applies to both values for leakage discharge tested. Both the average error and the standard deviation for these configurations are small. All realizations from this configuration satisfy the criterion for noticing the leakage from the piezometer data;
2. It is unnecessary to place piezometers with a mutual distance of only 4 meters since some configurations requiring less piezometers are available that predict the location of a leakage with sufficient or even more accuracy;
3. Configuration I accurately predicts the location of the leakage. This configuration has piezometers with a mutual distance of 12 meter which are placed at 8 meters distance from the diaphragm wall. Both the average error and the standard deviation are small, and their sum is about 1.5 meters. A disadvantage is the small possibility that this configuration fails the criterion for noticing the leakage from the piezometer data.

5.2.5. Results on the clay layer

Tables 5.9 and A4.6 show the following results for the clay layer (K=0.03 m/day):

1. Configuration D is the optimal configuration for the clay layer. It has piezometers at 4 meters from the wall which have a mutual distance of 4 meters. Both the average error and the standard deviation of the realizations are small for this configuration. All realizations from this configuration satisfy the criterion for noticing the leakage from the piezometer data;
2. Configuration E, in which piezometers have a mutual distance of 8 meters and are located at 4 meters from the diaphragm wall, on average satisfies the criterion for localizing the leakage. But since the individual realizations have a relatively high standard deviation, there is a possibility that this configuration fails to localize it. The criterion for noticing the leakage from the piezometer data is met;
3. A row of piezometers that is located at 8 meters from the diaphragm wall is too distant to accurately predict the location of a leakage. Also the standard deviation for such configurations is high. The criterion for noticing the leakage from the piezometer data fails in all but one of the realizations.

5.3. Discussion

5.3.1. The usefulness of ordinary kriging

Ordinary kriging has been used for the interpolation of piezometer data. Ordinary kriging is an interpolation procedure that is developed for the prediction of parameter values that are realizations of a wide sense stationary random function. This means that the mean of the random function is spatially constant, but this is obviously not the case when a leakage occurs: a leakage typically is a non-stationary process. Therefore, no statistical conclusions can be drawn from the prediction results in this research. This implies that the predicted head values along the diaphragm wall are biased rather than unbiased and that the calculation of the variance of the prediction error is nonsensical. Therefore, the use of these statistics is not attempted in this research.

Still, despite the lack of statistical meaning for non-stationary processes, ordinary kriging is an interpolation procedure that predicts the parameter value at some location, using parameter values at nearby locations that are weighted by their respective distance. This procedure is applied to all scenarios and configurations in the same way, so that any systematic error in the procedure cancels out. Only prediction results that are obtained by this procedure with the same systematic error are mutually compared. No meaningful value is attributed to the numerical value of the kriging results at locations along the diaphragm

wall, only the location where it is minimal has been searched for. So, despite the lack of statistical meaning of the prediction, ordinary kriging is still a spatial interpolation process that can be used for the purpose of this research.

5.3.2. The selection of semivariogram parameter values

The major range is taken to be 100 meters in all scenarios, which is the length of the diaphragm wall. In most of the realizations, the effect of the leakage could be seen in all piezometers close to the diaphragm wall, although the drawdown was only a single centimeter in some of them. The piezometer data along the diaphragm wall are all dropping due to the same cause, which is the leakage. Therefore, the major range is taken to be the length of the diaphragm wall, since piezometer data are still correlated over this distance. The nugget variance in the semivariogram model is taken to be only about ten percent of the variance of the heads of a specific realization. This is because the main reason for spatial head variations is the leakage, which is a process that has effects at a scale larger than the mutual distance between adjacent piezometers. Biases in piezometer measurements, which are small scale errors, may occur. But when assuming that these are non-systematic, the errors of several measurements that contribute to the kriging prediction may cancel. A small nugget variance accounts for this.

Some random samples among the configurations of scenario 1 showed that the values for major range, partial sill variance and nugget variance used in the kriging procedure are sensible: when the values for major range, partial sill variance and nugget variance were calculated by ArcGIS rather than manually entered, the kriging values did change. But the location along the diaphragm wall where the predicted head value was minimal either did not change or shifted away from the location of the leakage that was set in Modflow. So the manual input of values for major range, partial sill variance and nugget variance increased, or at least did not deteriorate, the result for a specific piezometer configuration.

5.3.3. Timely identifying a leakage from piezometer data

In some configurations applied at realizations of some scenarios, the data from the piezometers constituting this specific configuration do not yet identify the occurrence of a leakage anyway (apart from its location) at the time at which the data were exported from Modflow (see Table 5.2). The criterion for timely noticing a leakage fails when an insufficient head gradient is calculated from the piezometer data. The inability to notice a leakage at all especially applies for configurations P, Q and R, in which the piezometers are located relatively distant from the diaphragm wall. Also the configurations representing some rows of piezometers perpendicular to the diaphragm wall (configurations J through O) do not generally meet this criterion. Using these configurations, one would need some more time to observe that a leakage is occurring, after which its location can be determined by kriging. This is not assumed to negatively influence the kriging results since the pattern of isohypses does not heavily change over time in this stadium. Only the head value corresponding to each isohypse decreases over time. Yet, the sooner one notices a leakage the better it is, so another configuration is preferred.

5.3.4. Accuracy of the results for ordinary kriging

The overall accuracy of the individual errors given in Tables A4.1 through A4.6 is conservatively taken to be 0.5 meter, though some of these individual errors could be obtained more accurately. The overall accuracy of individual errors is determined by the accuracy with which the minimum of the curves resulting from the kriging predictions could be read in Excel (see Figure 5.9). The reading from these results for all 18 configurations of each realization is manually done. Since the results of 5 realizations of each scenario are averaged and the inaccuracy can be assumed to be non-systematically, the values for the average error in Tables 5.4 through 5.9 can be appreciated to be more accurate.

5.3.5. Interpretation of the results for ordinary kriging

A specific piezometer configuration is considered as 'satisfactory' for localizing a leakage when the average error of 5 realizations is less than 1.5 meters. Since a typical width of an element of a diaphragm wall is 3 meters, a piezometer configuration with an error of less than 1.5 meter can predict at which transition between wall elements a leakage is occurring.

The obvious result (see Tables 5.4 through 5.9) that a piezometer configuration is more suitable to localize a leakage when piezometers are placed in a row parallel rather than perpendicular to the diaphragm wall is not surprising: the leakage is located at the wall, so it has to be squeezed between two piezometers on a line parallel to the wall which measure the largest head drop. The installation of additional piezometers perpendicular to the wall does not contribute to this squeezing. Still, such an additional piezometer may be useful when another piezometer in its row is defect.

5.3.6. Limitations of the software used

In order to obtain the head drawdown at a given time that was obtained in Modflow, the leakage discharge in a real field situation would be smaller than the leakage discharge that was modeled in Modflow (see Table 5.2). This is due to the fact that the leakage in Modflow is modeled by a well. In the model, this well not only discharges water from outside the building site, but also from inside the building site. Therefore, the time period after the occurrence of the leakage at which the piezometer data from Modflow cause to suspect a leak is overestimated: in reality one would need some less time to observe that a leakage is occurring, given the leakage discharge in Table 5.2. Yet, there is no reason to assume that interpolating piezometer data in a field situation at an earlier time negatively influences the kriging results, since the pattern of isohypses does not heavily change over time in this stadium. Only the head value corresponding to each isohypse decreases over time.

Two piezometers on the line adjacent to the diaphragm wall had to be added to the piezometers corresponding to each specific piezometer configuration (see Figure 5.1 and Figure 5.8). This is because only interpolation and no extrapolation can be done in ArcGIS, but predicted piezometer data in the area directly adjacent to the diaphragm wall are searched for in this research. By adding these two piezometers in ArcGIS, the line adjacent to the wall is now included in the area that is interpolated. In a field situation, one would either have to include these two piezometers on top of the piezometers corresponding to the desired configuration, or one would need software that can extrapolate using kriging. The addition of these two piezometers in this research is not assumed to noticeably influence the kriging results since these piezometers are distant from large parts of the diaphragm wall where leakages are simulated.

5.4. Conclusions

Research question (2): what piezometer configuration is optimal for localizing a theoretical leak in a diaphragm wall?

Answer: the optimal configurations for localizing a leakage for each of the three values for conductivity that are tested are given in Table 5.10. In all scenarios, the optimal configuration is a row of piezometers with a specific mutual distance that have a specific distance from the diaphragm wall.

Conductivity (m/day)	Optimal configuration	Distance piezometers from diaphragm wall (m)	Mutual distance piezometers (m)

30	E	4	8
1	E or H	4 or 8	8
0.03	D	4	4

Table 5.10. Optimal piezometer configurations.

The results from the research presented in this chapter show that optimization of the piezometer configuration can be used as a tool for passive leak detection. Using only five realizations for each scenario already indicates which piezometer configurations are most useful for localizing a leakage. This passive method for testing the state of a diaphragm wall has therefore been proved useful.

5.5. Recommendations

An extension of this research is recommended if the risk by leakages at a real building site has to be analyzed. The sensitivity (step size) in the research presented in this chapter is 4 meters: the mutual distance between piezometers in a row was a multiple of 4 meters. Also the distance of each row of piezometers from the diaphragm wall was a multiple of 4 meters, except for the row at 2 meters from the wall. It is recommended to improve this sensitivity by decreasing this distance of 4 meters when analyzing a real building site. Also, it is recommended to test more than five realizations for a real building site. By doing so, outliers in the results for prediction error are more averaged so that the predictive value is increased.

The procedure presented for localizing a theoretical leakage in a theoretical aquifer is expanded to the real building site of Vijzelgracht Station in the next chapter. Retrospectively, the optimal piezometer configuration that best had been used at this site is searched for. The approach is the same as in this chapter: a large number of theoretical leakages are successively simulated in a model in Modflow. Ordinary kriging is applied with the aim of reproducing the respective locations of the leakage by different piezometer configurations.

6. OPTIMIZING PIEZOMETER CONFIGURATION FOR LOCALIZING A THEORETICAL LEAK IN THE DIAPHRAGM WALL OF VIJZELGRACHT STATION

6.1. Method

The rationale behind the method applied in this chapter is the same as in the previous chapter. But in this chapter, it is applied to Vijzelgracht Station rather than to some imaginary building site. Based on the results of the previous chapter and practical limitations at Vijzelgracht Station, another selection of piezometer configurations is tested for their ability to localize a theoretical leak that typically could have occurred in the diaphragm wall of Vijzelgracht Station during proceedings at this building site.

6.1.1. Simulating a leakage at Vijzelgracht Station in Modflow

A model of Vijzelgracht Station is made in Modflow. The model area is 750 meters northing by 525 meters easting. The building site is placed in the centre of this area. The grid size inside and just outside the building site is 0.5 by 0.5 meters. The grid size in some wider area around it is 5 by 5 meters and the grid size at more distant locations is 25 by 25 meters. An overview of the model grid drawn over a city map is shown in Figure 6.1.

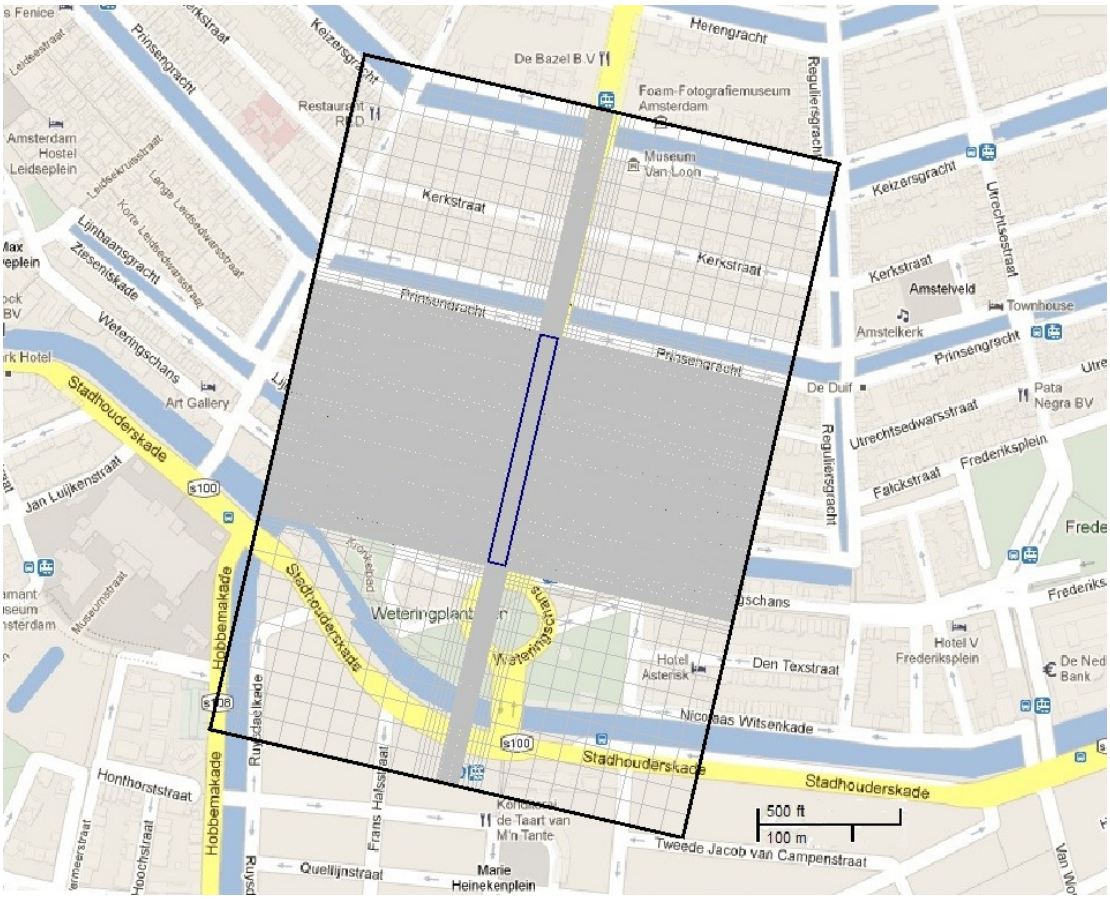

Figure 6.1. Model area of Vijzelgracht Station. The black contour indicates the model borders; the blue contour indicates the location of the diaphragm wall.

The model consists of 12 layers. An overview of the model parameter values that are used for these layers is given in Table 6.1. The parameter values in this table are adopted from Duineveld (2009) and Salet (2010). Compared to the soil structure given in Table 3.1, layer 10 is divided into two separate layers in Modflow since the diaphragm wall of Vijzelgracht Station reaches to a depth of NAP-45 meter, which is somewhere halfway this clay layer.

All layers are taken to be isotropic, so no distinction is made between horizontal and vertical conductivity.

Layer	Depth (m)		Name/material	Conductivity (m/day)	Initial head (m)	Specific storage (m^{-1})	Effective porosity (-)
	from	*to*					
1	0	-3	sand	5	-0.85	0.0001	0.25
2	-3	-6.5	clay	0.0007	-0.85	0.0001	0.25
3	-6.5	-9	sand	5	-0.85	0.0001	0.25
4	-9	-12	clay	0.00075	-0.85	0.0001	0.25
5	-12	-14	first sand layer	30	-2.35	0.0001	0.25
6	-14	-17	alleröd	0.12	-2.5	0.0001	0.25
7	-17	-25	second sand layer	30	-2.6	0.0001	0.25
8	-25	-41	clay	0.005	-2.8	0.0001	0.25
9	-41	-43	'tussenzandlaag'	0.3	-3	0.0001	0.25
10	-43	-45	clay	0.002	-3	0.0001	0.25
11	-45	-50.5	clay	0.002	-3	0.0001	0.25
12	-50.5	-55	third sand layer	30	-3	0.0001	0.25

Table 6.1. Parameters for the model of Vijzelgracht Station in Modflow.

All cells bordering the model area are assigned a constant head value, and layer 12 is wholly assigned a constant head value. All constant head values are given by the initial head values for each respective layer. The diaphragm wall is modeled in layers 1 through 10 and has a thickness of 2 grid cells, which corresponds to 1 meter. The hydraulic resistance of the diaphragm wall is 1200 days (Salet, 2010) so the horizontal and vertical conductivity of cells at the location of the diaphragm wall are taken to be 1/1200 = 0.000833 m/day. Other parameter values for these cells are equal to those given in Table 6.1 for each respective layer.

A leakage is assumed to occur in the first sand layer, so it is modeled in layer 5 in Modflow. Two real, major leakages occurred in this layer in 2008 (Salet, 2008). The leakage modeled in this research is assumed to occur at the stage when the building site is dug up to the bottom of layer 3. Grid cells of the top three layers inside the building site are therefore set inactive. In the real situation where the proceedings have progressed up to this stage, the heads in the first and second sand layer (layers 5 and 7) will have to be decreased to prevent the risk of uplifting of the bottom of the building site. The model accounts for this by drains placed in layers 5 and 7 along the diaphragm wall, with a mutual distance of 20 meters. The hydraulic conductance of each drain is set to 1000 m^2/day and their elevation is set to -14 meters, which is the bottom level of layer 5.

Some heterogeneity in layer 5, in which the leakage occurs, is modeled. The values for horizontal and vertical conductivity are generated by the Field Generator in Modflow. The average conductivity is taken to be 30 m/day, its standard deviation is 3 m/day and the correlation length of the conductivity field is taken to be 0.05 along both the rows and columns of the model grid.

Two models are used for obtaining the resulting head drawdown due to a leakage:

1. A model as described above is run with the time parameter set to steady-state. This model results in the steady-state head distribution prior to the occurrence of a leakage;
2. The head values resulting from the steady-state model are saved and imported as initial head values in a second model. Besides these initial head values, the model

parameters are equal to those in the steady-state model. But now the time parameter is set to transient and a leakage is modeled to occur in the first time period. This time period has a time length of 12 hours, divided into 24 time steps. Therefore, data on drawdown evolution over time are available in intervals of half an hour.

The leakage is simulated by placing a well in one of the outer cells of the western part of the diaphragm wall in layer 5. This well simulates a leakage that is assumed to occur at the transition of two elements of the diaphragm wall. The volume of the leakage discharge through such a joint is calculated by putting some typical numbers in Equation (3.9) (see Section 3.4 and Appendix 1):

1. The joint length (l) of the leaking transition is taken to be 2 meters. This is the thickness of layer 5;
2. The joint width (b) is taken to be 0.04 meters. This width is determined by the grain size distribution of the concrete used for constructing the diaphragm wall elements (Bhageloe, 2004);
3. The diaphragm wall thickness (d) is taken to be 1.2 meters (Dijk, 2008);
4. It is assumed that the joint is filled with sand from the aquifer. Therefore, the hydraulic conductivity (K) is taken to be 30 m/day, which is the average conductivity of layer 5;
5. The head difference (H) over the wall prior to the leakage is taken to be 11.4 meters. The head in layer 5 outside the diaphragm wall in the steady-state model is -2.6 meters. Inside the building site, the head in layer 5 is -14 meters. So the difference between these is 11.4 meters.

When these five numbers are used in Equation (3.9), a leakage discharge of 24 m^3/day results. The well that is placed in Modflow to simulate the leakage is therefore assigned a discharge value of 24 m^3/day.

Three rows of piezometers are placed in Modflow, west of the building site. These piezometers record the head drawdown over time during the leakage. Each row consists of 130 piezometers with a mutual distance of 2 meters. The three rows of piezometers are placed at 4, 6 and 8 meters from the diaphragm wall respectively. Two additional piezometers are placed at the line adjacent to the diaphragm wall: one is located 2 meters south from its southern border while another is located 2 meters north from its northern border. By doing so, ArcGIS will include the area directly adjacent to the diaphragm wall in the kriging procedure.

The head data from all these piezometers are saved and exported from Modflow to ArcGIS after two hours after the occurrence of the leakage. Ten different locations (realizations) for the leakage are successively modeled and their respective piezometer data are exported to ArcGIS. The location of each of these ten realizations is given in Table 6.2. These locations are expressed in meters north of the southwestern corner of the diaphragm wall.

Realization	Location (m)
1	104.25
2	183.25
3	50.75
4	220.75
5	155.25
6	79.75
7	22.25

8	202.75
9	230.25
10	128.25

Table 6.2. The location of the leakage for each of the ten realizations in Modflow. Locations are expressed in meters north of the southwestern corner.

As in the previous chapter, the data of each piezometer configuration are tested on their ability to notice that a leakage is occurring anyway. A realization of a specific piezometer configuration is considered as 'satisfactory' *for noticing the occurrence of a leakage* when a hydraulic head gradient of at least 0.0025 is observed between any two piezometers in this configuration. A specific piezometer configuration is considered as 'satisfactory' *for localizing a leakage* when the average error of the 10 realizations is less than 1.5 meters. The 'error' is defined as the distance between the modeled (known) location of the leakage in Modflow and the location predicted by the kriging procedure.

6.1.2. Interpolation of head measurements at Vijzelgracht Station by ordinary kriging in ArcGIS

A total number of 18 subsets of the piezometer data that are exported by Modflow are used in ArcGIS for ordinary kriging. Each of these 18 subsets corresponds to a specific piezometer configuration. In all these configurations, a row of piezometers with a specific mutual distance is placed at a specific distance from the diaphragm wall. An overview and description of these 18 configurations is given in Table 6.3.

Piezometer configuration	**Description of piezometer configuration**	
	Distance between row and wall (m)	*Mutual piezometer distance (m)*
A	4	6
B	4	8
C	4	10
D	4	12
E	4	14
F	4	16
G	6	6
H	6	8
I	6	10
J	6	12
K	6	14
L	6	16
M	8	6
N	8	8
O	8	10
P	8	12
Q	8	14
R	8	16

Table 6.3. Description of 18 piezometer configurations. In all configurations, a row of piezometers is placed along the diaphragm wall.

In ArcGIS, ordinary kriging is performed on these 18 configurations. An exponential semivariogram model is applied for the kriging procedure. The value for major range is taken to be 200 meters. This is the maximum length along the diaphragm wall where the hydraulic head is still noticeably affected by the leakage after two hours after its occurrence. The variance of the head measurements for each realization in Modflow is calculated in Excel. This variance is the sum of the partial sill variance and the nugget

variance (Pardo-Igúzquiza, 2012). The nugget variance is taken to be about ten percent of the partial sill variance. The values for nugget variance and partial sill variance for the semivariogram model for all individual realizations are given in Appendix 3.2.

A part of the kriging results of each configuration is exported to Excel, namely the interpolation results over the line that is directly adjacent to the diaphragm wall. These data points are plotted versus their corresponding position along the wall. The position along the diaphragm wall where the curve belonging to a specific configuration has its minimum is interpreted as the location of the leakage that is predicted by that specific configuration. This location is compared to the known location of the leakage that was set in Modflow. The error belonging to a specific configuration is taken to be the difference between the location of the leakage that was set in Modflow and the location that is read from the curve that is obtained after the kriging procedure. The average error of 10 realizations is calculated in order to compensate for measurement errors and for dependency of the result on the location of the leakage that was set in Modflow.

6.2. Results

An example of the visual result from the kriging procedure for Vijzelgracht Station in ArcGIS is shown in Figure 6.2. This example shows the result for realization 1 (see Table 6.2). In this specific example, the kriging result from configuration M (see Table 6.3) is shown, together with its corresponding piezometer configuration. The western border of the diaphragm wall is indicated by the blue line. The location of the leakage is indicated by X.

A legend is also shown in Figure 6.2, but the absolute numerical results for head values along the wall are not useful. This is because the head drawdown along the wall is underestimated by the kriging procedure: the results from the kriging procedure indicate that the largest drawdown in the area is obtained at the location of the piezometer that has the largest drawdown. At any other location, the predicted drawdown is less than at the location of this piezometer. This is obviously not true for a real leakage at Vijzelgracht Station, since the largest drawdown occurs directly adjacent to the diaphragm wall, at the location of the leakage. Therefore, the predicted head values that result from kriging are only used to predict the location of the leakage, which is at the minimum head value.

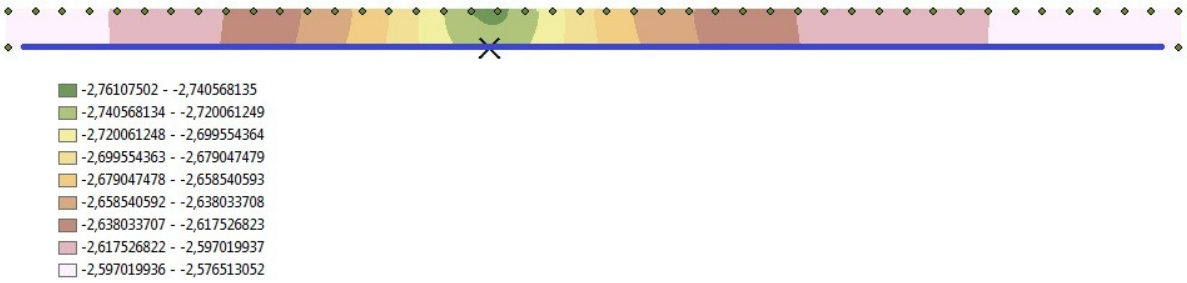

Figure 6.2. Example of a visual result from the kriging procedure. Head values are given in meters above NAP.

Figure 6.3 shows an example of a diagram that is drawn in Excel after importing the predicted head values from the kriging procedure. It shows the predicted head values at the line that is directly adjacent to the diaphragm wall. This specific diagram shows the results from the kriging procedure of piezometer configuration A through R of realization 1. As discussed in the previous paragraph, the predicted head values underestimate the real drawdown along the diaphragm wall at the location of the leakage.

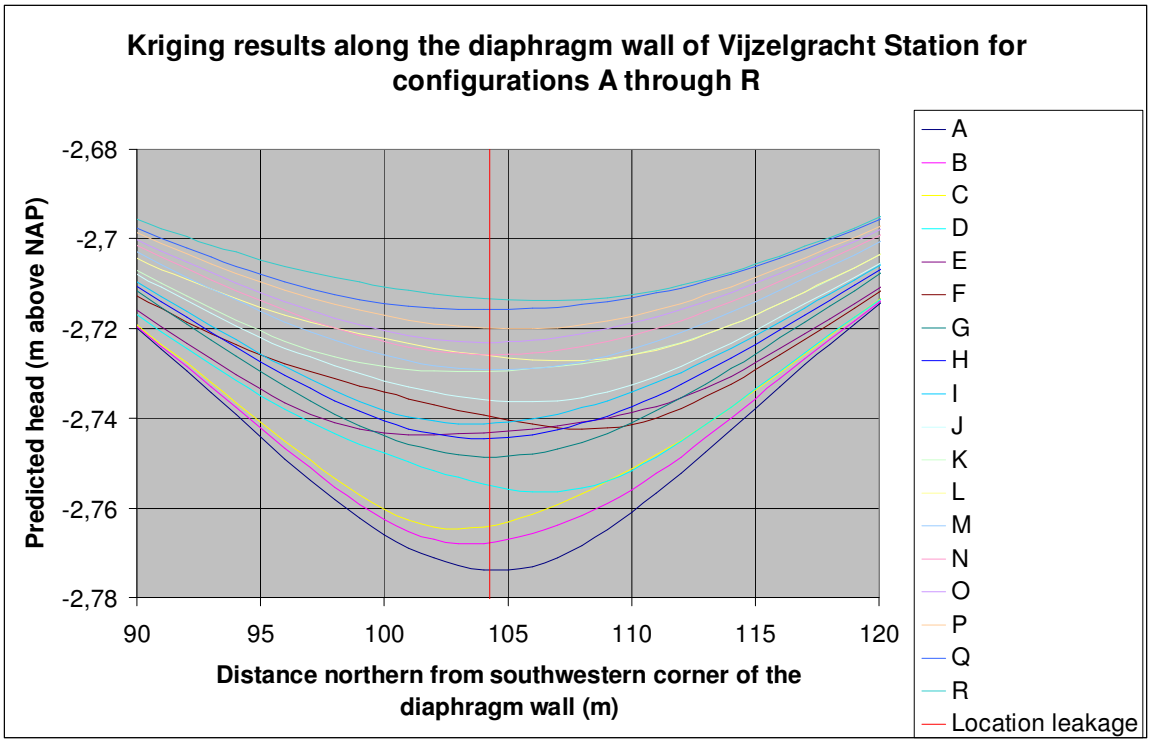

Figure 6.3. Result for the kriging procedure of piezometer configuration A through R of realization 1. The red line indicates the location of the leakage that was set in Modflow.

The average error of 10 realizations for all configurations is given in Table 6.4. Also the standard deviation of these 10 realizations and the number of piezometers required for each configuration are given in Table 6.4. The individual errors that resulted for all 18 configurations for all 10 realizations are given in Table A4.7 in Appendix 4.2. In all piezometer datasets underlying these realizations, a head gradient between two piezometers of at least 0.0025 is observed. So the criterion for noticing the occurrence of the leakage is satisfied for all realizations.

Piezometer configuration	Number of piezometers	Average error of ten realizations (m)	Standard deviation of ten realizations (m)
A	44	0.38	0.24
B	33	0.68	0.35
C	26	0.98	0.42
D	22	1.88	0.66
E	19	2.58	1.05
F	17	2.70	1.30
G	44	0.55	0.55
H	33	0.53	0.32
I	26	0.63	0.21
J	22	1.35	0.77
K	19	1.93	1.04
L	17	2.13	1.23
M	44	0.85	0.69
N	33	0.70	0.57
O	26	0.78	0.55
P	22	1.18	0.96
Q	19	1.55	1.22

R	17	1.70	1.38

Table 6.4. Average error and standard deviation of ten realizations at Vijzelgracht Station.

Tables 6.4 and A4.7 show the following results:

1. Configuration I is the optimal configuration for Vijzelgracht Station. Piezometers in this configuration have a mutual distance of 10 meters and are placed in a row at 6 meters distance from the diaphragm wall. At all 10 individual realizations in this research, the accuracy criterion at this realization is amply satisfied;
2. Configuration P on average predicts the location of the leakage with sufficient accuracy. Piezometers in this configuration have a mutual distance of 12 meters and are placed at a row at 8 meters distance from the diaphragm wall. However, the standard deviation in this configuration is relatively large and at 4 out of 10 individual realizations, the accuracy criterion is not met;
3. It is unnecessary to place piezometers with a mutual distance of only 6 or 8 meters since some configurations requiring less piezometers are available that predict the location of a leakage with sufficient or even more accuracy;
4. Configurations in which piezometers have a mutual distance of 14 or 16 meters do not sufficiently accurate predict the location of a leakage.

6.3. Discussion

The discussions in Sections 5.3.1, 5.3.2 and 5.3.6 are also applicable to Chapter 6, but are not repeated here. These three sections deal with the usefulness of ordinary kriging, the selection of semivariogram parameter values and the limitations of the software used respectively. Other discussions from Section 5.3 are inapplicable or require some adjustments for this chapter.

6.3.1. The tested piezometer configurations

As a consequence of the results from the previous chapter, no piezometer configurations were tested in which piezometers are placed in rows perpendicular to the diaphragm wall of Vijzelgracht Station. Placing piezometers in some rows perpendicular to a diaphragm wall generally appeared to poorly predict the location of the leakage.

Vijzelgracht Station is built below a street bordered by houses and other buildings. The distance between the building site and these buildings is generally up to 8 meters, and at some locations it is even less. Therefore, configurations in which piezometers are located more distant than 8 meters from the building site were not applied in this chapter.

From the results, it can be read that the average error for configurations with piezometers having a relatively large mutual distance decreases when placing this row more distant from the diaphragm wall (see configurations F, L and R in Table 6.4), although the realizations constituting this average value have a high standard deviation. Therefore, an interesting question is whether this trend of a decreasing average error continues for rows of piezometers at even larger distance from the wall. This question is not answered by the research in this chapter since such configurations are not feasible at Vijzelgracht Station. The results from the previous chapter, though, indicate that there is some optimal distance for a row of piezometers from the diaphragm wall, given their mutual distance. The results from the previous chapter show that this optimal distance is less then 12 meters from the wall for all aquifer parameter values tested.

6.3.2. Comparison of the results from a theoretical building site and Vijzelgracht Station

The leakage occurring at Vijzelgracht Station was modeled in a sand layer with a thickness of 2 meters and an (average) conductivity of 30 m/day. These aquifer parameters are equal to those used in scenario 1 in the previous chapter. Four piezometer configurations were

tested in both models: these are rows of piezometers located at 4 and 8 meters from the diaphragm wall respectively. For both of these distances, a mutual piezometer distance of both 8 and 12 meters was applied. Two similarities in the results from the previous chapter and this chapter are:

1. When piezometers are placed at 4 meters from the diaphragm wall, increasing their mutual distance from 8 to 12 meters clearly increases the average error;
2. When piezometers with a mutual distance of 12 meters are placed, increasing their distance from the diaphragm wall from 4 to 8 meters clearly decreases the average error.

Also two dissimilarities can be observed:

1. When piezometers with a mutual distance of 8 meters are placed, increasing their distance from the diaphragm wall from 4 to 8 meters leaves the average error at Vijzelgracht Station about unchanged, while this somewhat increases the average error in scenario 1 in the previous chapter;
2. When piezometers are placed at 8 meters from the diaphragm wall, increasing their mutual distance from 8 to 12 meters leads to some increased average error at Vijzelgracht Station but it leads to some decreased average error in scenario 1 in the previous chapter.

6.3.3. The effect of a leakage near the corner of a diaphragm wall

In two of the ten realizations used in the model of Vijzelgracht Station, a leakage was modeled to occur near the corner of the diaphragm wall. In realization 7, it was modeled at 22.25 meters from the southwestern corner and in realization 9, it was modeled at 23.25 meters from the northwestern corner. If the results from these two realizations would be excluded from the total set of 10 realizations used in this chapter, the average error for many configurations would substantially decrease. This especially applies for configurations in which the mutual distance between piezometers is 12 meters or more. Also, this decrease in error is enhanced for configurations in which piezometers are placed relatively distant from the diaphragm wall. These effects may imply that it is best to choose a configuration with piezometers relatively distant from the wall and with a relatively large mutual distance over the large middle part of the diaphragm wall, while the opposite applies for piezometers placed near its corner.

6.3.4. Accuracy of the results for ordinary kriging

The error for the individual results of each realization (see Appendix 4.2) was manually read in Excel and could generally be read with an accuracy of 0.25 meter. Yet, some of these results could only be read with an accuracy of 0.5 meter. These less accurate results determine the overall accuracy, which is therefore conservatively assumed to be 0.5 meter. Since the results of 10 realizations are averaged, the values for the average error in Table 6.4 can be appreciated to be more accurate.

6.4. Conclusions

Research question (3): what piezometer configuration is optimal for localizing a theoretical leak in the diaphragm wall of Vijzelgracht Station?

Answer: the optimal configuration at Vijzelgracht Station is a row of piezometers with a mutual distance of 10 meters that are placed at 6 meters from the diaphragm wall. This conclusion is based on a typical leakage occurring in the first sand layer.

The research presented in this chapter has shown that optimizing the piezometer configuration at a real building site can be applied as a tool for passive leak detection. The results show that it is worthwhile to spend some effort on making a model and applying

some simulations on it to find the optimal piezometer configuration. By doing so, some time and money is invested to reduce the risk of larger scale damage due to the inability to notice and localize a leakage.

6.5. Recommendations

As an extension of the research presented in this chapter, optimizing the piezometer configuration should be done in all aquifers that are intersected by the diaphragm wall. If possible, the results from all aquifers should be combined so that an optimal multi-level piezometer configuration is obtained.

It is recommended to place a dense piezometer network in Modflow so that configurations with varying piezometer density can be tested. In addition, this allows one to easily extend the set of tested piezometers configurations if an optimal configuration is not yet obtained by the initial results. The research on Vijzelgracht Station showed that an optimal configuration can be indicated with an accuracy of 2 meter: both the optimal distance of a row of piezometers from the diaphragm wall and their optimal mutual distance can be indicated with this accuracy. Increasing the piezometer density in Modflow enables the testing of more configurations, which may improve this accuracy.

As discussed in Section 6.3.3, the optimal piezometer configuration over the large middle part of the diaphragm wall is not necessarily the optimal configuration for localizing a leakage at a location that is near its corner. So when applying some optimization analysis on a model of a building site, one should search for the optimal configuration at both the middle part and the part in the vicinity of the corner. Also the location of the transition from one type of optimal leakage detection to the other should be searched for.

7. ACTIVELY TESTING THE WATERTIGHTNESS OF A WATER RESISTANT SCREEN BY GEOELECTRICAL MEASUREMENTS: A CASE STUDY

7.1. Method

The geoelectrical measurement method, discussed in Section 3.6, is applied in a field situation in the province of Overijssel in the Netherlands. A passenger tunnel below a railway station is constructed at this location. One or more leakages are present in the sheet piling framing the building site. At this site, the leakage impedes the completion of the proceedings, but does not cause a risk to the surrounding area. The leakage was observed by an artesian well that appeared in the building site with a severe discharge rate of about ten cubic meters per hour. Previous analysis at the site has indicated that a leakage in the sheet piling is located below the level of a thin natural aquitard that is present below the excavation level in the building site. This aquitard previously hindered the water to enter the building site from below, but an opening appeared at the location of a weakness in it, enabling the water to enter the building site. The geoelectrical measurements on this location were performed in December 2012 and were preceded by an earlier geoelectrical measurement at a neighboring part of the sheet piling.

A schematic map of the site is shown in Figure 7.1. The measurements are performed in two stages, so two grids of measurement sensors are successively installed. The first and the second grid comprise 67 and 53 measurement sensors respectively. There is a small overlap between the two grids, as can be seen in Figure 7.1. The part of the sheet piling that is tested, indicated by the black line, is less than ten percent of the total length of sheet piling at this building site. Sensors are placed at every lock between the elements of the sheet piling, which have a width of 60 centimeters. The sensors that are not placed along the wall have a mutual distance of 1.8 or 2 meters.

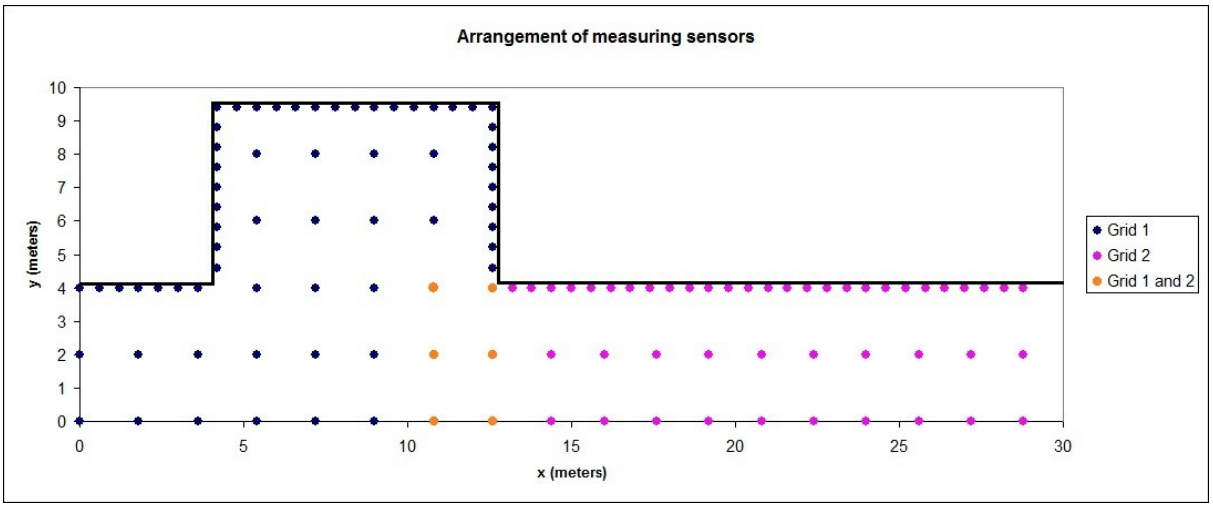

Figure 7.1. Sensor grids. The black line indicates the sheet piling.

Figure 7.2 shows a part of the tested area with the installed measurement equipment. This figure shows the upper left corner of the cove that can be seen in Figure 7.1. Since most of the floor of the building site is already concreted, sensors placed on many of the grid points are not in direct contact with the soil. Therefore, small holes are drilled in the concrete, which are filled with wet bentonite. The sensors are placed on top of these bentonite filled drill holes, as can be seen in Figure 7.2. The figure also shows a large yellow well that drains the leakage water from the building site and a couple of smaller drainage wells along the sheet piling.

Figure 7.2. Measurement equipment installed at the building site.

The series of voltages applied to the source pole outside the building site comprises a self potential measurement and five subsequent measurements with voltages of 25, 50, 75, 150 and 250 millivolts respectively. For each voltage, ten measurements are done with a time interval of 14 seconds. After the measurements in the first grid area are completed, the equipment is moved to the second grid area and there the same measurement procedure is performed. For all voltages, the results from the second last out of ten measurements are used for further analysis: the potential values for all sensors are spatially interpolated and the resulting equipotential maps are interpreted.

7.2. Results

The data obtained from the geoelectrical measurements result in an equipotential map for each of the values for voltages applied. Figure 7.3 shows one such resulting map, in this case, it is the map corresponding to the results from the 50 millivolts measurements. This value is chosen here because the final map that is delivered to the client (see figure 7.4) is based on this map. Also, as discussed in Section 3.6, maps based on measurements using a relatively high voltage may be less appropriate when a steel sheet piling is tested. Figure 7.3 shows some blue colored regions, which are the locations where an anomalous high potential value is measured, indicating a potential leakage.

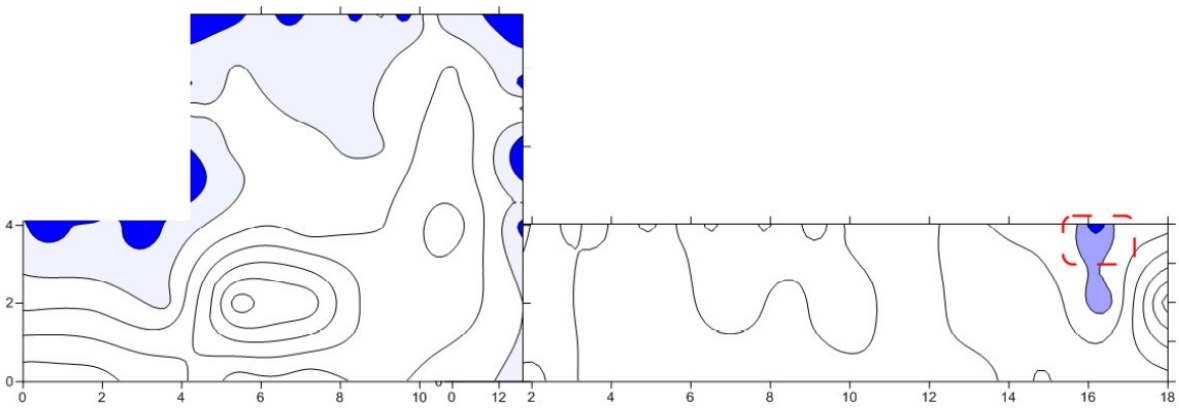

Figure 7.3. Equipotential map based on the 50 millivolts measurements.

Figure 7.4 shows the map that is presented to the client. It is equal to Figure 7.3, but it is extended with additional field information and the results of the interpretation. The yellow circle in the figure indicates the location of a metal object, which clearly disturbs the pattern of equipotential lines. The left part of the sheet piling is interpreted to have leakages at many of the locks. Though some of the filled contours in the figure indicate which locks are most likely to be leaking, the map is not fully decisive. An additional difficulty in the interpretation of these results is the presence of many small drainage wells, as can be seen in Figure 7.4. These wells may disturb the pattern of equipotential lines. Since this part of the sheet piling cannot be interpreted on the scale of individual locks, and, moreover, keeping in mind the previous results of geoelectrical measurements at this building site, the whole left part of the area is interpreted as leaking. Therefore, the leakage is probably best repaired by implementing measures at all locks in this area.

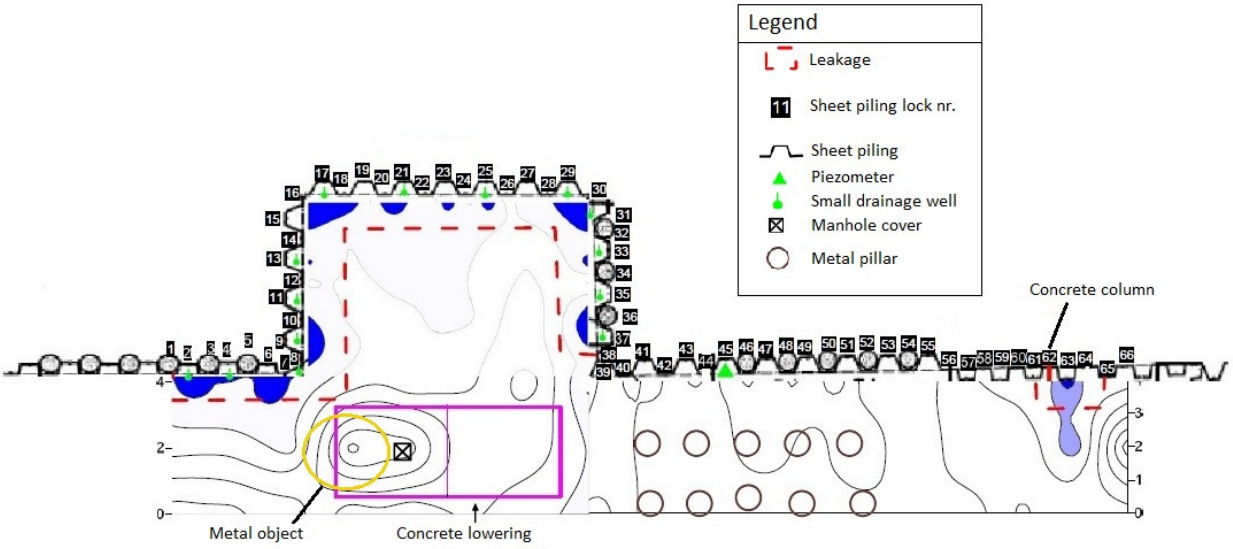

Figure 7.4. Equipotential map extended with field information and interpretations.

A more local leakage is observed in Figure 7.4 at the right part of the sheet piling, at lock number 63. This leakage was previously assumed to be located at lock number 62. A concrete column was constructed against this lock on the inside of the building site, but the leakage was not resolved by it. The geoelectrical measurements have identified that a leakage is still present at lock number 63, which may have been enhanced by the repair of lock number 62, so measures are to be taken here.

7.3. Discussion

The geoelectrical measurement method discussed in this chapter results in an equipotential map from which the two-dimensional position of a leakage ideally is read. But on top of this result, when testing a sheet piling, one may be interested in the depth and length of the leaking lock, as well as in the leakage discharge rate per leaking lock.

The geoelectrical method generally does not indicate the depth of a leakage, but the arrangement of the equipment can be adjusted in order to get some indications on this: if multiple piezometers with screens at different depths are available outside the building site, a series of measurements can be performed in which the piezometer used for the source pole is changed for each measurement. The resulting equipotential maps may show different results for each piezometer used, so a rough estimate of the depth of the leakage may be read from it. Nevertheless, it is not generally useful to know the depth of the leakage: when a repair is required, this is usually done in a thorough way over the whole depth of the water resistant screen. The depth of the leakage is therefore not relevant; identifying its two-dimensional location suffices.

Geoelectrical measurements can not yet be used to calculate the leakage discharge rate. This would require a quantitative relationship between electrical conductance and flow velocity of groundwater, on which no literature is available. Knowledge on the leakage discharge per lock may be useful when many neighboring locks are suspected to be leaking, as is the case in the left part of the map in Figure 7.4. Since one may doubt if a leakage is really present at every single lock in this area, it is useful to know at which of the locks the leakage discharge is highest. These locks can be repaired first, after which another measurement can test whether or not the leakage is sufficiently reduced. On the other hand, when a leakage can be attributed to only one or a few locks, as is the case in the right part of the map in Figure 7.4, knowledge on the leakage discharge is less relevant: the leaking locks have to be repaired anyhow, independent of their exact discharge rate.

As discussed, the results shown in the left part of Figure 7.4 cannot identify which individual locks are leaking, but its right part is much more distinct. This higher distinctiveness is also observed from several other equipotential maps that have resulted from measurements at other building sites. Therefore, the low distinctive result shown in the left part of Figure 7.4 is more the exception than the rule for geoelectrical measurements.

7.4. Conclusions

Research question (4): how can geoelectrical measurements be used to actively test the watertightness of a water resistant screen?

Answer: the watertightness of a water resistant screen framing a building site can be actively tested by installing a dense grid of sensors inside the building site. These sensors measure the change in the geoelectrical potential of the groundwater as a consequence of a voltage applied to an electrical source pole that is placed in a piezometer outside the building site. Leakages in the water resistant screen can be interpreted from the map showing the interpolated sensor potential values from these geoelectrical measurements.

7.5. Recommendations

The geoelectrical measurement method developed by Texplor GmbH has proven to be a useful tool for leak detection in water resistant screens. It has been successfully applied at many locations. The performance of the measurements takes relatively little time and is relatively straightforward. The method is therefore recommended for leak detection at underground building sites.

APPENDIX 1 DERIVATION OF THE EQUATION FOR THEORETICAL LEAKAGE DISCHARGE

Bruggeman et al. (1985) have derived an analytical method to calculate the leakage discharge (Q [L^3/T]) through a joint between parts of a diaphragm wall. Their analysis starts with a derivation for the head in a rectangular opening in an impermeable wall with constant heads at each side of the wall. The head is assumed to be constant over the area of the opening. The head difference between opening and one side of the wall (h) and volume density flux (q [L/T]), obtained after some Fourier transforms, is given by

$$h = \frac{2q}{\pi K}\left[\frac{l}{2}\cdot \sinh^{-1}\left(\frac{b}{l}\right)+\frac{b}{2}\cdot \sinh^{-1}\left(\frac{l}{b}\right)+\frac{b^3+l^3-(b^2+l^2)^{3/2}}{6\cdot b\cdot l}\right] \qquad \text{(A1.1)}$$

In this equation, K is hydraulic conductivity, l is the length of the opening and b is the width of the opening. The transition from a rectangular opening to an elongated joint is made by defining

$$\alpha = l/b \qquad \text{(A1.2)}$$

This ratio of opening length to opening width can be taken very large in order to calculate the leakage flux through a joint. Define $S = l\cdot b$ to be the surface area of the joint. The relationship between the head difference over the wall (H=2h) and volume flux or leakage flux (Q=S·q [L^3/T]) is then given by

$$H = \frac{Q}{\pi\cdot K\cdot\sqrt{S}}F(\alpha) \qquad \text{(A1.3)}$$

In which the dimensionless function F is given by

$$F(\alpha) = \frac{2}{\sqrt{\alpha}}\left[\alpha\cdot\sinh^{-1}\left(\frac{1}{\alpha}\right)+\sinh^{-1}(\alpha)-\frac{(1+\alpha^2)^{3/2}-(1+\alpha^3)}{3\cdot\alpha}\right] \qquad \text{(A1.4)}$$

Rewriting Equation (A1.3) while using H=2h and Q=S·q gives

$$Q = \frac{h\cdot S}{F(\alpha)\sqrt{S}/(2\pi K)} \qquad \text{(A1.5)}$$

In this form, the entrance resistance (w_e) and outflow resistance (w_o) are given by the denominator:

$$w_e = w_o = \frac{F(\alpha)\sqrt{S}}{2\pi K} \qquad \text{(A1.6)}$$

The flow resistance through the opening of the wall with thickness d is given by

$$w_f = \frac{d}{K} \qquad \text{(A1.7)}$$

Now the total resistance for water entering, flowing through and leaving the joint is given by

$$w_t = w_e + w_f + w_o = \frac{1}{K}\left(\frac{F(\alpha)\sqrt{S}}{\pi} + d\right) \qquad \text{(A1.8)}$$

So finally, the relation between Q and H can be written as

$$Q = \frac{S \cdot H}{w_t} = \frac{K \cdot S \cdot H}{d + \frac{F(\alpha)\sqrt{S}}{\pi}} \qquad \text{(A1.9) = (3.9)}$$

APPENDIX 2 DERIVATION OF THE EQUATION FOR LINEAR FLOW IN A BUILDING SITE

Equation (3.4) has to be modified in order to make it useful for linear flow in the case study in Chapter 4. The length unit used by Pujades et al. (2012) is taken to be d_{dw}, which is the distance between the two diaphragm walls and so the width of the excavation site. The aquifer thickness, which is another space dimension, is already included in Equation (3.4) via transmissivity, which is hydraulic conductivity times aquifer thickness. Now two expressions for well discharge Q can be derived:

$$Q = 2s_p \sqrt{\frac{S_{aq} T_{aq}}{\pi \cdot t}} \cdot d_{dw} \qquad \text{(A2.1)}$$

$$Q = -S_{aq} \cdot A \cdot \frac{dh}{dt} \qquad \text{(A2.2)}$$

Equation (A2.1) follows from Equation (3.4) and Equation (A2.2) follows immediately from the definition of the aquifer storage coefficient when discharge Q is constant and A is the aquifer area affected by the average drawdown.

Before putting Equations (A2.1) and (A2.2) equal, it is assumed that:

$$\left. \frac{A(r)}{d_{dw}} \right|_r = 2r \qquad \text{(A2.3)}$$

This assumption is only valid when pumping well and piezometer are approximately lined up along the diaphragm wall. This is the case for the pumping test considered in the case study. A few notes that support the validity of Equation (A2.3) are first that the dimensions are right; a second note is that the dependence of r still had to be included in Equations (A2.1) and (A2.2). A third note is that a linear flow situation is dealt with, so a linear relation is the simplest assumption. Putting Equations (A2.1) and (A2.2) equal while using Equation (A2.3) leads to:

$$\frac{\partial h}{\partial t}(r,t) = -s_p \sqrt{\frac{T_{aq}}{S_{aq} \cdot \pi \cdot r^2 t}} \qquad \text{(A2.4)}$$

Integrating this leads to the expression for linear flow:

$$h(r,t) = -s_p \sqrt{\frac{T_{aq} \cdot t}{S_{aq} \cdot \pi \cdot r^2}} + h(r, t=0) \qquad \text{(A2.5) = (4.2)}$$

APPENDIX 3 PARTIAL SILL VARIANCE AND NUGGET VARIANCE

3.1. Partial sill variance and nugget variance for Chapter 5

The partial sill variance and nugget variance for all realizations in Chapter 5 are given in Table A3.1.

Scenario		Realization 1	Realization 2	Realization 3	Realization 4	Realization 5
1	partial sill (m^2)	0.0008	0.00072	0.0008	0.00082	0.0008
	nugget (m^2)	0.000076	0.00008	0.000072	0.000087	0.000088
2	partial sill (m^2)	0.00085	0.0008	0.00085	0.0008	0.0008
	nugget (m^2)	0.000093	0.000082	0.000089	0.00009	0.000093
3	partial sill (m^2)	0.0011	0.00125	0.00115	0.0012	0.00108
	nugget (m^2)	0.000157	0.000135	0.000141	0.000115	0.000102
4	partial sill (m^2)	0.00077	0.00073	0.00065	0.00075	0.00075
	nugget (m^2)	0.000075	0.000071	0.000075	0.000082	0.000065
5	partial sill (m^2)	0.00083	0.00083	0.0011	0.00082	0.00096
	nugget (m^2)	0.000085	0.000088	0.000112	0.000076	0.000086
6	partial sill (m^2)	0.00028	0.00029	0.00026	0.00028	0.00035
	nugget (m^2)	0.00003	0.000033	0.000022	0.000022	0.000031

Table A3.1. Semivariogram parameters for Chapter 5.

3.2. Partial sill variance and nugget variance for Chapter 6

The partial sill variance and nugget variance for all ten realizations in Chapter 6 are given in Table A3.2.

Realization	Partial sill variance (m^2)	Nugget variance (m^2)
1	0.0024	0.000297
2	0.0022	0.000207
3	0.0025	0.000294
4	0.002	0.000198
5	0.0023	0.000252
6	0.0026	0.00026
7	0.0022	0.000148
8	0.0022	0.000123
9	0.0019	0.000166
10	0.0024	0.000249

Table A3.2. Semivariogram parameters for Chapter 6.

APPENDIX 4 ORDINARY KRIGING RESULTS FOR ALL INDIVIDUAL REALIZATIONS

4.1. Ordinary kriging results for individual realizations in Chapter 5

Tables A4.1 through A4.6 show the individual errors of each configuration for all realizations of all six scenarios respectively. The number of piezometers in the head of these tables is abbreviated by '# pm'. Also the average error for each configuration is given. A cell that is highlighted in yellow indicates that a specific configuration in a specific realization fails to notice that a leakage is occurring from the piezometer data. A realization of a specific piezometer configuration is considered as 'satisfactory' *for noticing the occurrence of a leakage* when a hydraulic head gradient of at least 0.0025 is observed between any two piezometers in this configuration. For scenario 6, in which a leakage occurs in a clay layer (K=0.03 m/day), this value for hydraulic gradient is taken to be 0.001.

Conf.	# pm.	Error for each of 5 realizations (m)					Average error (m)
		1	2	3	4	5	
A	27	0.5	0.5	0.5	0.5	0.5	**0.5**
B	14	1.5	0.5	0.5	1.5	1.5	**1.1**
C	9	3.5	4.5	0.5	2.5	3	**2.8**
D	27	0.5	1.5	0.5	0.5	0.5	**0.7**
E	14	0.5	1.5	0.5	1.5	0.5	**0.9**
F	9	2.5	3.5	0.5	1.5	0.5	**1.7**
G	27	0.5	1.5	0.5	0.5	0.5	**0.7**
H	14	2	1.5	0.5	1.5	0.5	**1.2**
I	9	1.5	1.5	0.5	0.5	0.5	**0.9**
J	9	3.5	12.5	9.5	2.5	8.5	**7.3**
K	15	3.5	12.5	9.5	2.5	8.5	**7.3**
L	12	4.5	11.5	2.5	6.5	8.5	**6.7**
M	20	4.5	11.5	2.5	6.5	7.5	**6.5**
N	18	2.5	2.5	3.5	2.5	4.5	**3.1**
O	30	2.5	2.5	4	2.5	4.5	**3.2**
P	27	1	1	0.5	2	0	**0.9**
Q	14	2.5	3.5	0.5	2	0.5	**1.8**
R	9	1.5	7.5	0.5	1.5	0.5	**2.3**

Table A4.1. Results for scenario 1.

Conf.	# pm.	Error for each of 5 realizations (m)					Average error (m)
		1	2	3	4	5	
A	27	0.5	0.5	0.5	0	0.5	**0.4**
B	14	0.5	1.5	0.5	0.5	1.5	**0.9**
C	9	3.5	3.5	4.5	1.5	1.5	**2.9**
D	27	0.5	0.5	0.5	0.5	0.5	**0.5**
E	14	0	1.5	1.5	0.5	0.5	**0.8**
F	9	2.5	1	3.5	0.5	1.5	**1.8**
G	27	0.5	0.5	2	2.5	0.5	**1.2**
H	14	1	1	2.5	2.5	0.5	**1.5**
I	9	2.5	0.5	3	2	0.5	**1.7**
J	9	3.5	4.5	15	6.5	10	**7.9**
K	15	3.5	4.5	15	6.5	10.5	**8.0**
L	12	2.5	3.5	10	4.5	3.5	**4.8**
M	20	2.5	3.5	10	4.5	3.5	**4.8**
N	18	3.5	1.5	0.5	3.5	4.5	**2.7**
O	30	3.5	1.5	0.5	3.5	4.5	**2.7**
P	27	1.5	1	2.5	8.5	1	**2.9**

Q	14	2.5	3.5	1.5	3.5	1	**2.4**
R	9	2.5	1	1	3.5	1	**1.8**

Table A4.2. Results for scenario 2.

Conf.	**# pm.**	**Error for each of 5 realizations (m)**					**Average error (m)**
		1	2	3	4	5	
A	27	0.5	0.5	0.5	0.5	0.5	**0.5**
B	14	1.5	1.5	1.5	1.5	1.5	**1.5**
C	9	0.5	1.5	1.5	2.5	4.5	**2.1**
D	27	0.5	0.5	0.5	0.5	1.5	**0.7**
E	14	0.5	0	0.5	1.5	0.5	**0.6**
F	9	0.5	1	1.5	1.5	4.5	**1.8**
G	27	0.5	2	0.5	1	2	**1.2**
H	14	0.5	2	0.5	1.5	2	**1.3**
I	9	0.5	1.5	0.5	0.5	2.5	**1.1**
J	9	1.5	9.5	10	2.5	12.5	**7.2**
K	15	1.5	9.5	10.5	2.5	12.5	**7.3**
L	12	6.5	3.5	3.5	6.5	10.5	**6.1**
M	20	7.5	3.5	3.5	6.5	10.5	**6.3**
N	18	5	4	4.5	2.5	1.5	**3.5**
O	30	5	4.5	4.5	2.5	1.5	**3.6**
P	27	0.5	7.5	1	1.5	1	**2.3**
Q	14	1	3	1	2	0.5	**1.5**
R	9	1	2.5	1	1.5	2.5	**1.7**

Table A4.3. Results for scenario 3.

Conf.	**# pm.**	**Error for each of 5 realizations (m)**					**Average error (m)**
		1	2	3	4	5	
A	27	0.5	0.5	0.5	0.5	0.5	**0.5**
B	14	1.5	1.5	1.5	0.5	1.5	**1.3**
C	9	2.5	2.5	4.5	3.5	2.5	**3.1**
D	27	0.5	0.5	0.5	0.5	0.5	**0.5**
E	14	0.5	0.5	0.5	0.5	0.5	**0.5**
F	9	1.5	2.5	3.5	2.5	1.5	**2.3**
G	27	0.5	0	1.5	1.5	0.5	**0.8**
H	14	0	0.5	1	0.5	0.5	**0.5**
I	9	1	1	1.5	1.5	1.5	**1.3**
J	9	0.5	7.5	12	4.5	1.5	**5.2**
K	15	0.5	7.5	12	4.5	1.5	**5.2**
L	12	6.5	5.5	10.5	1.5	3.5	**5.5**
M	20	6.5	5.5	10.5	1.5	3.5	**5.5**
N	18	4.5	5.5	1.5	4.5	2.5	**3.7**
O	30	4.5	5.5	1.5	4.5	2.5	**3.7**
P	27	0.5	0	1	2.5	0.5	**0.9**
Q	14	0.5	0.5	2.5	1.5	1.5	**1.3**
R	9	1	0.5	7	1.5	1.5	**2.3**

Table A4.4. Results for scenario 4.

Conf.	**# pm.**	**Error for each of 5 realizations (m)**					**Average error (m)**
		1	2	3	4	5	
A	27	0.5	0.5	0.5	0.5	0.5	**0.5**

B	14	1.5	0.5	1.5	1.5	1.5	**1.3**
C	9	2.5	0.5	3	3.5	3.5	**2.6**
D	27	0.5	0.5	0.5	0.5	0.5	**0.5**
E	14	1	0	1.5	0.5	0.5	**0.7**
F	9	1.5	0.5	0.5	1	2.5	**1.2**
G	27	0	0.5	3.5	0.5	0.5	**1.0**
H	14	0	0.5	1	0.5	0.5	**0.5**
I	9	1	0.5	1.5	0.5	1	**0.9**
J	9	7.5	7.5	6.5	8.5	8.5	**7.7**
K	15	7.5	7.5	6.5	8.5	8.5	**7.7**
L	12	0.5	5.5	0.5	8.5	2.5	**3.5**
M	20	0.5	5.5	0.5	7.5	2.5	**3.3**
N	18	1.5	3.5	5.5	4.5	0.5	**3.1**
O	30	1.5	3.5	5.5	4.5	0.5	**3.1**
P	27	0	2	4.5	0.5	0.5	**1.5**
Q	14	0	1.5	1.5	1	0.5	**0.9**
R	9	0.5	1	2	1	0.5	**1.0**

Table A4.5. Results for scenario 5.

Conf.	**# pm.**	**Error for each of 5 realizations (m)**					**Average error (m)**
		1	2	3	4	5	
A	27	0.5	0.5	0.5	0.5	0.5	**0.5**
B	14	1.5	2.5	2.5	0.5	2.5	**1.9**
C	9	1.5	2.5	3.5	4	4	**3.1**
D	27	0.5	0	0	0.5	0.5	**0.3**
E	14	1	2	1.5	0.5	1.5	**1.3**
F	9	1.5	2.5	2	3.5	2	**2.3**
G	27	0	2	4.5	1.5	0	**1.6**
H	14	0	2.5	2	1.5	0.5	**1.3**
I	9	0	3	2	2.5	0	**1.5**
J	9	10.5	10	3.5	4.5	4.5	**6.6**
K	15	11	10	3.5	4.5	4.5	**6.7**
L	12	0.5	8	1.5	1.5	3.5	**3.0**
M	20	0.5	8.5	1.5	1.5	3.5	**3.1**
N	18	2.5	1.5	6.5	4.5	1.5	**3.3**
O	30	2.5	1.5	6.5	4.5	1.5	**3.3**

Table A4.6. Results for scenario 6. Scenarios P through R were not applied in this scenario.

4.2. Ordinary kriging results for individual realizations in Chapter 6

Table A4.7 shows the individual errors for all realizations of all configurations tested at Vijzelgracht Station. The average error is given in the last column.

Conf.	**R.1**	**R.2**	**R.3**	**R.4**	**R.5**	**R.6**	**R.7**	**R.8**	**R.9**	**R.10**	**Av.**
A	0.5	0.25	0.25	0.75	0.25	0.25	0.75	0.5	0.25	0	**0.38**
B	1	0.75	1	0.25	0.75	0.75	0.5	0.25	0.25	1.25	**0.68**
C	1.25	1	1	0.25	1.5	1.25	0.5	0.75	0.75	1.5	**0.98**
D	2.25	2.25	1.75	2.75	0.75	2.25	1.75	0.75	2.25	2	**1.88**
E	2.5	1.25	3.25	2	1.25	3	4.25	2.5	4	1.75	**2.58**
F	3.75	3.25	3	0.5	1.75	1.75	5	2.25	3.75	2	**2.70**
G	0	0.25	0.5	1.75	0.25	0	1	0.5	1	0.25	**0.55**

H	0.25	0.5	0.5	0.75	0	0.5	1	0.25	1	0.5	**0.53**
I	0.5	0.75	0.75	0.25	1	0.5	0.75	0.75	0.5	0.5	**0.63**
J	1.5	1.75	0.75	2.5	0.25	1.25	1.75	0.25	2.25	1.25	**1.35**
K	1	1.25	2.5	1	1	2.25	3.75	1.75	3.5	1.25	**1.93**
L	3	1.5	2.25	0.25	1.75	1.25	4.5	1.75	3.5	1.5	**2.13**
M	0.25	0.5	1	2	0.5	0.25	1.75	0.75	1.5	0	**0.85**
N	0.25	0.5	0.5	1.25	0.25	0.25	1.75	0.5	1.5	0.25	**0.70**
O	0	0.75	0.75	1	0.75	0.25	1.75	0.75	1.5	0.25	**0.78**
P	1	1.5	0	2.5	0.25	0.75	2.5	0.25	2.25	0.75	**1.18**
Q	0	1	2	0.5	1	1.25	3.75	1.5	3.5	1	**1.55**
R	2.25	0.25	1.25	0.75	1	1	4.5	1	3.75	1.25	**1.70**

Table A4.7. Individual errors (m) and average value (m) of all ten realizations at Vijzelgracht Station.

APPENDIX 5 REFERENCES

Bhageloe, G.S., 2004. Waterbezwaar ten gevolge van lekkende diepwandvoegen door ontbrekende stop-ends.

Bierkens, M.F.P., Geer van, F.C., 2011. Course reader Stochastic Hydrology GEO4-4420.

Bruggeman, G., Braadbaart, F., 1985. Lek door civieltechnische schermen; analyse en berekening. pt/c 40, 19-25.

Dijk, J.P., 2008. Plan repareren voegen - Projectbureau NZL.

Duineveld, M., 2009. Praktijkproef Vijzelgracht; meetresultaten en interpretatie.

Heinz, A., Geutebrück, E., 2011. FGM® quality system procedure; manual.

Jonker, J.H., 2010. Handboek diepwanden; ontwerp en uitvoering. COB/CUR-publicatie 231.

Kurtulus, B., Flipo, N., Goblet, P., Vilain, G., Tournebize, J. Tallec, G., 2011. Hydraulic head interpolation in an aquifer unit using ANFIS and ordinary kriging. Computational Intelligence 343, 265-276.

Pardo-Igúzquiza, E., Dowd, P.A., 2012. Comparison of inference methods for estimating semivariogram model parameters and their uncertainty: The case of small data sets. Computers & Geosciences, http://dx.doi.org/10.1016/j.cageo.2012.06.002.

Pujades, E., Carrera, J., Vázquez-Suñé, E., Jurado, A., Vilarrasa, V., Mascuñano-Salvador, E., 2012. Hydraulic characterization of diaphragm walls for cut and cover tunnelling. Engineering Geology 125, 1-10.

Pujades, E., 2012. Email on November 9th 2012.

Renard, P., Glenz, D., Mejias, M., 2008. Understanding diagnostic plots for well-test interpretation. Hydrogeology Journal 17, 589-600.

Salet, T.A.M., 2008. Incident lekkage diepwand Vijzelgracht.

Salet, T.A.M., 2010. Fijnkalibratie model station Vijzelgracht na uitvoeren praktijkproeven tussenzandlaag.